

Token-Efficient Change Detection in LLM APIs

Timothée Chauvin ^{*1} Clément Lalanne ^{†23} Erwan Le Merrer ¹ Jean-Michel Loubes ⁴⁵³ François Taïani ¹
Gilles Tredan ⁶

Abstract

Remote change detection in LLMs is a difficult problem. Existing methods are either too expensive for deployment at scale, or require initial white-box access to model weights or grey-box access to log probabilities. We aim to achieve both low cost and strict black-box operation, observing only output tokens.

Our approach hinges on specific inputs we call Border Inputs, for which there exists more than one output top token. From a statistical perspective, optimal change detection depends on the model’s Jacobian and the Fisher information of the output distribution. Analyzing these quantities in low-temperature regimes shows that border inputs enable powerful change detection tests.

Building on this insight, we propose the Black-Box Border Input Tracking (B3IT) scheme. Extensive in-vivo and in-vitro experiments show that border inputs are easily found for non-reasoning tested endpoints, and achieve performance on par with the best available grey-box approaches. B3IT reduces costs by 30 \times compared to existing methods, while operating in a strict black-box setting.

1. Introduction

LLM APIs are increasingly embedded in high-impact applications, such as software engineering (Zheng et al., 2025), yet users have no guarantee that the model behind an endpoint remains unchanged. Providers may modify models for safety updates, cost optimization, or infrastructure changes, often without notice. Quietly deploying quantized versions to reduce costs, for instance, could degrade performance on tasks users depend on. Such changes are not hypothetical: Grok on X suffered three incidents in 2025 where

^{*}First author, method and experiments. [†]First author, theory and analysis. ¹Université de Rennes, Inria, CNRS/IRISA (Rennes, France) ²Univ Toulouse, INUC, UT2J, INSA Toulouse, TSE, CNRS, IMT, Toulouse, France ³ANITI Toulouse ⁴Inria ⁵Regalia ⁶LAAS, CNRS, (Toulouse, France). Correspondence to: Timothée Chauvin <<https://tchauvin.com/contact>>.

Preprint. February 12, 2026.

modified system prompts were deployed due to rogue employees or bad updates (Babuschkin, 2025; xAI, 2025a;b). Anthropic experienced infrastructure bugs in 2025 that degraded Claude’s responses, which remained undetected for weeks despite affecting 16% of Claude Sonnet 4 requests at peak (Anthropic, 2025).

Several change-detection methods have been proposed (Gao et al., 2025; Bai et al., 2025; Gubri et al., 2024; Chauvin et al., 2026). However, they face a fundamental tension between access requirements and cost. White-box methods like ESF (Bai et al., 2025) and TRAP (Gubri et al., 2024) craft sensitive inputs using model internals (embeddings, gradient-based optimization), limiting their use to known models. Grey-box methods like LT (Chauvin et al., 2026) require log-probabilities, which are available only on a fraction of public endpoints. Fully black-box approaches like MET (Gao et al., 2025) avoid these requirements but demand many queries to the tracked model, making continuous monitoring prohibitively expensive.

We introduce B3IT (*Black-Box Border Input Tracking*), a change-detection method that operates in a strict black-box setting, observing only output tokens, while achieving accuracy and cost efficiency comparable to grey-box approaches. Our key insight, brought by a theoretical analysis, is that at low temperature, inputs where two tokens are nearly tied as the top prediction (“border inputs”) become extremely sensitive detectors. In other words, even tiny model changes can dramatically alter the output distribution. We show theoretically that this sensitivity diverges as temperature tends to zero, exhibiting a phase transition between detectable and undetectable regimes.

B3IT exploits this phenomenon: it discovers border inputs through black-box sampling, then monitors for changes by comparing output distributions. Surprisingly, border inputs are easy to find on most production models. The result is a method that detects subtle changes at 1/30th the cost of alternatives, enabling large-scale continuous and cost-effective API monitoring.

Contributions. (1) We establish theoretical foundations for change detection in LLMs, revealing a phase transition at low temperature that enables high-sensitivity detection

without model access. **(2)** We propose B3IT, a practical black-box method that identifies border inputs and uses them for efficient change detection. **(3)** We validate B3IT *in vitro* on TinyChange (Chauvin et al., 2026), achieving detection performance comparable with grey-box methods at 1/30th the cost of the next best black-box baselines. **(4)** We demonstrate B3IT *in vivo* on 93 endpoints (64 models, 20 providers), showing broad applicability for continuous monitoring.

Roadmap. Section 2 describes our system model. Section 3 presents the theoretical analysis underpinning the B3IT method, which we describe in Section 4 and evaluate in Section 5.

Code. All our code is open-source at github.com/timothee-chauvin/token-efficient-change-detection-llm-apis.

2. System model

In this paper, we take the perspective of an unprivileged user facing a black-box API exposing an LLM f_θ , where $\theta \in \Theta$ denotes the (unknown) model parameters. The user can only submit queries (x, T) for some input $x \in \mathcal{X}$ and temperature $T \in \mathbb{R}^+$, and collect the answer $f_\theta(x, T)$.

Change detection. We consider a two-stage interaction: an *initialization stage* and a *detection stage*. Let θ_0 denote the model parameters during initialization and θ_1 during detection. The change detection problem consists in deciding whether $\theta_0 = \theta_1$, as in prior work (Gao et al., 2025; Chauvin et al., 2026). Formalized as a hypothesis test, let $H_0 := \theta_0 = \theta_1$ (the model hasn’t changed) versus $H_1 := \theta_0 \neq \theta_1$ (the model has changed).

In this endeavor, we are interested in two key quantities:

- **Detector accuracy:** we want to minimize false positives (incorrectly detecting a change) and false negatives (missing actual changes). Formalizing a test as a (possibly randomized) function ϕ taking values in $[0, 1]$, we therefore seek to minimize $\mathbb{P}(\phi = 1|H_0) + \mathbb{P}(\phi = 0|H_1)$.
- **Cost:** for wide-scale monitoring of LLM APIs, detecting changes should induce a minimal cost. This is especially true of the detection stage, which is run repeatedly.

Types of changes. Deployed LLMs can undergo many kinds of modifications: fine-tuning (full or Low-Rank Adaptation (Hu et al., 2022)), quantization, model distillation, system prompt changes, or further Reinforcement Learning. Infrastructure can also affect outputs: CUDA versions, GPU selection, compiler optimizations, or routing errors directing requests to misconfigured servers (Anthropic, 2025). The

intensity of any such modification determines detection difficulty; our focus is on query-efficient detection, regardless of the change’s origin or intensity.

For the theoretical analysis, we model parameter changes as $\theta_1 := \theta_0 + \epsilon h$ where $h \in \mathbb{S}^{q-1}$ is a unit direction and ϵ controls magnitude. This local perturbation model enables tractable analysis via the Local Asymptotic Normality framework (Section 3). In experiments, we directly evaluate on realistic updates (fine-tuning, pruning, etc.) across a range of change magnitudes, and on live LLM APIs.

Single-token perspective. Our analysis focuses on the first output token from a single query. While approaches such as MET (Gao et al., 2025) leverage multiple output tokens, inter-token dependencies complicate the analysis substantially. However, multiple queries from different prompts can be combined for improved performance, which we demonstrate experimentally.

3. Theoretical analysis and guidelines

Building on optimal change detection in the sense of Neyman–Pearson (Neyman & Pearson, 1933), we exhibit a new phase-transition phenomenon for LLMs (Theorem 3.3). At temperature $T \ll 1$, inputs where two or more tokens share the maximal logit become extremely sensitive to parameter changes: we call these *Border Inputs* (BIs). This result provides the theoretical foundation for B3IT, which we introduce in Section 4.

3.1. Rationale

Testing whether two LLMs differ reduces to testing whether they induce different probability distributions over tokens. We focus on the distribution of the first generated token and, for analytical tractability, assume independence across generations.

Since the token distribution is finite, the problem formally reduces to multinomial hypothesis testing, a classical setting with an extensive literature directly studying the problem, or related ones such as estimation (Balakrishnan & Wasserman, 2019; Berrett & Butucea, 2020; Cai et al., 2024; Aliakbarpour et al., 2024; Cressie & Read, 2018; Barron, 1989; Kim, 2019; Acharya et al., 2019; 2018; Kairouz et al., 2016; Acharya et al., 2017a;b; Louati, 2025). However, these generic results do not account for the structure of LLMs, or for the ability to design informative input prompts. We therefore analyze how prompt choice and sampling temperature shape sensitivity to model perturbations, ultimately identifying BIs as appealing test inputs.

3.2. The Local Asymptotic Normality Framework

Let $\mathbf{p} = (p_1, \dots, p_{d-1}) \in (0, 1)^{d-1}$ denote the reduced parametrization of the categorical output distribution, with $p_d := 1 - \sum_{i=1}^{d-1} p_i > 0$. The vector \mathbf{p} models the output distribution over tokens, where d is the vocabulary size. We adopt this reduced parametrization to isolate the free variables. Querying the model n times on the same input yields i.i.d. samples $Y_1, \dots, Y_n \sim \mathbf{p}$.

We define the reduced empirical frequency estimator $T_n := \hat{\mathbf{p}} := (\hat{p}_1, \dots, \hat{p}_{d-1}), \hat{p}_j := \frac{1}{n} \sum_{i=1}^n \mathbf{1}\{Y_i = j\}$. This estimator is unbiased and satisfies $\text{Cov}_{\mathbf{p}}(T_n) = \frac{1}{n} F(\mathbf{p})$, where $F(\mathbf{p}) := \text{diag}(\mathbf{p}) - \mathbf{p}\mathbf{p}^T$ is the inverse of the Fisher information matrix of the distribution \mathbf{p} . Since T_n is a sufficient statistic, it contains all the information needed to construct optimal tests.

Consider two sets of model parameters θ_0 and θ_1 , inducing token distributions \mathbf{p}_0 and \mathbf{p}_1 , respectively. By the Central Limit Theorem (see (van der Vaart, 1998), Example 2.18), the statistic T_n admits the asymptotic Gaussian approximation $T_n \sim \mathcal{N}(\mathbf{p}_k, \frac{1}{n} F(\mathbf{p}_k)), k \in \{0, 1\}$.

Let $\theta \in \Theta \subset \mathbb{R}^q$ denote the model parameters, let x_{test} be the prompt used for testing, and define the reduced output map $g(\theta, x_{\text{test}}) := f(\theta, x_{\text{test}})_{1:(d-1)} \in (0, 1)^{d-1}$. We consider a perturbation of the parameters of the form $\theta \mapsto \theta + \epsilon h, h \in \mathbb{S}^{q-1}$, and write $\mathbf{p}_1 := g(\theta + \epsilon h, x_{\text{test}}), \mathbf{p}_0 := g(\theta, x_{\text{test}})$.

In order to better understand the regime under which we analyze tests, we first explain what goes wrong without the right approach. In practice, we aim to detect very small parameter changes, i.e. $\epsilon \ll 1$. If $\epsilon \rightarrow 0$ (used to model a small perturbation) too quickly, and for the sake of reasoning, assume the above Gaussian approximation for T_n holds, the distributions of T_n under \mathbf{p}_0 and \mathbf{p}_1 become indistinguishable, making testing impossible. We analyze the problem in this regime not as an extra assumption, but as the natural framework that makes the testing problem meaningful.

A meaningful theory emerges by considering small parameter perturbations in the Local Asymptotic Normality (LAN) regime (see (van der Vaart, 1998), Chapters 7 and 16), which we now introduce. This framework is central in statistics, as it characterizes the regime in which hypothesis testing is neither trivial nor impossible.

Assuming $g(\theta, x_{\text{test}})$ is differentiable with respect to θ , we consider local perturbations of the form $\epsilon_n = \frac{s}{\sqrt{n}}$ for $s \in \mathbb{R}$ fixed, and obtain the expansion $\mathbf{p}_n := \mathbf{p}_{\epsilon_n} = \mathbf{p}_0 + \epsilon_n Jh + r_n$, where $J := \nabla_{\theta} g(\theta, x_{\text{test}})$ is the Jacobian of the reduced output distribution w.r.t. the model parameters, and $\sqrt{n} \|r_n\| \rightarrow 0$. This corresponds to a small parameter perturbation in direction h at the critical rate that preserves

nontrivial asymptotic effects.

Leveraging the perspective of this regime leads to the following result, which quantifies the asymptotic power of optimal tests.

Theorem 3.1 (Optimal Tests in the LAN Regime). *Let $\alpha \in (0, 1)$. If (ϕ_n) is a sequence of tests such that, for every n , ϕ_n is the test with the lowest Type-II error among all tests with Type-I error at most α in testing \mathbf{p}_0 vs \mathbf{p}_n , then*

$$\text{Type-II}(\phi_n) \rightarrow \mathbb{P} \left(\mathcal{N}(0, 1) \leq Q_{\alpha} - \sqrt{s^2 \text{SNR}^2(h)} \right) \quad (1)$$

where $\text{SNR}^2(h) := h^T (J^T F(\mathbf{p}_0)^{-1} J) h$, and $\text{Type-II}(\phi_n)$ refers to the error of ϕ_n under \mathbf{p}_n , and where Q_{α} is the quantile of order $1 - \alpha$ of $\mathcal{N}(0, 1)$.

Proof. See Section B.2. □

This result is central to our theory, as it shows that the viability of the optimal (and thus any) test is entirely characterized by a single scalar quantity, $\text{SNR}^2(h)$, which captures the intrinsic difficulty of the testing problem: the higher it is, the easier the test. It conveniently takes the form of a signal-to-noise ratio, where the signal is the change in intensity, and the noise comes from temperature sampling.

Takeaway. In the small-variation regime, optimal change detection is governed by three elements: the tampering direction h , the Jacobian of the model, and the Fisher information of the output token distribution, combined through the criterion $\text{SNR}^2(h)$. The Jacobian controls the signal: a large Jacobian amplifies how parameter perturbations affect the output distribution. The Fisher information controls the noise: a well-conditioned (low-variance) output distribution reduces sampling uncertainty and improves detectability.

Balancing these effects may seem difficult in a black-box setting. We show, however, that tuning the sampling temperature provides concrete control over this trade-off.

3.3. Decomposition for LLMs: exploiting the last layer

A key observation underlying our theory is that, for LLMs, the expression of $\text{SNR}^2(h)$ can be further simplified by making the transformer architecture explicit.

Let $r(\theta, x_{\text{test}}) \in \mathbb{R}^m$ denote the representation produced by the model up to the last layer. The final layer is a linear head (W, b) producing logits $z(\theta) = z(\theta, x_{\text{test}}) = Wr(\theta, x_{\text{test}}) + b \in \mathbb{R}^d$. Given a temperature $\tau > 0$, the output token distribution is computed as the softmax of the logits: $p_i^{(\tau)}(\theta) = \frac{\exp(z_i(\theta)/\tau)}{\sum_{j=1}^d \exp(z_j(\theta)/\tau)}$, for $i = 1, \dots, d$.

We will write $\mathbf{p}^{(\tau)}(\theta) \in \mathbb{R}^d$ for the full vector and $\mathbf{p}_{1:(d-1)}^{(\tau)}(\theta) \in \mathbb{R}^{d-1}$ for its reduced coordinates.

We define the full matrix $\Sigma(\mathbf{p}) := \text{diag}(\mathbf{p}) - \mathbf{p}\mathbf{p}^T \in \mathbb{R}^{d \times d}$, and recall the reduced matrix $F(\mathbf{p}_{1:(d-1)}) := \text{diag}(\mathbf{p}_{1:(d-1)}) - \mathbf{p}_{1:(d-1)}\mathbf{p}_{1:(d-1)}^T \in \mathbb{R}^{(d-1) \times (d-1)}$. We use these two different notations to better distinguish reduced coordinates from full coordinates.

We write the parameters as $\theta = (\theta_{\text{pre}}, W, b)$, where θ_{pre} collects all parameters before the head, so that $r(\theta, x_{\text{test}}) = r(\theta_{\text{pre}}, x_{\text{test}})$. We define $J_r(\theta_{\text{pre}}) := \frac{\partial r(\theta_{\text{pre}}, x_{\text{test}})}{\partial \theta_{\text{pre}}} \in \mathbb{R}^{m \times q_{\text{pre}}}$. Then the Jacobian of the logits w.r.t. the full parameter vector $J_z(\theta) \in \mathbb{R}^{d \times (q_{\text{pre}} + dm + d)}$ decomposes as $J_z(\theta) = \left[\underbrace{W J_r(\theta_{\text{pre}})}_{\in \mathbb{R}^{d \times q_{\text{pre}}}} \mid \underbrace{r(\theta_{\text{pre}}, x_{\text{test}})^T \otimes I_d}_{\in \mathbb{R}^{d \times (dm)}} \mid \underbrace{I_d}_{\in \mathbb{R}^{d \times d}} \right]$.

Finally, let $J^{(\tau)}(\theta) := \frac{\partial \mathbf{p}_{1:(d-1)}^{(\tau)}(\theta)}{\partial \theta} \in \mathbb{R}^{(d-1) \times (q_{\text{pre}} + dm + d)}$ be the Jacobian of the reduced output map.

Lemma 3.2 (SNR²(h) in LLMs). *For any $\tau > 0$,*

$$\text{SNR}^2(h) = \frac{1}{\tau^2} h^T \left(J_z(\theta)^T \Sigma \left(\mathbf{p}^{(\tau)}(\theta) \right) J_z(\theta) \right) h. \quad (2)$$

Proof. See Section B.3. \square

Although purely technical, this result is crucial to our theory: it renders the analysis tractable for LLMs, with the simplification of the inner inverse arising from the structure of the softmax layer, and enables the derivation of our main result.

3.4. The Zero-Temperature Limit

We now have all the ingredients to study the low-temperature regime and present our main theoretical result. Let $z := z(\theta)$ and define the set of maximizers $\mathcal{M} := \{i \in \{1, \dots, d\} : z_i = \max_{1 \leq j \leq d} z_j\}$, $k := |\mathcal{M}|$.

We further define $\Sigma_{\mathcal{M}}$ as the operator Σ applied to the probability vector assigning uniform mass to \mathcal{M} and zero mass elsewhere.

Theorem 3.3 (Phase Transition). *Depending on the value of k ,*

- If $k = 1$, then $\text{SNR}^2(h) \rightarrow 0$ as $\tau \rightarrow 0$.
- If $k \geq 2$, and if $h^T (J_z^T \Sigma_{\mathcal{M}} J_z) h \neq 0$, then $\text{SNR}^2(h) \rightarrow +\infty$ as $\tau \rightarrow 0$.

Proof. See Section B.4. \square

Remark 3.4 (On the condition $h^T (J_z^T \Sigma_{\mathcal{M}} J_z) h \neq 0$). At first glance, the condition $h^T (J_z^T \Sigma_{\mathcal{M}} J_z) h \neq 0$ may appear restrictive. However, as discussed in Section B.5, it holds for almost every direction h . In particular, if h is not

degenerate and is, for instance, modeled as a continuous random perturbation of the parameters, this condition is satisfied with probability one.

Takeaway. At very low temperature, detectability exhibits a sharp dichotomy. If the output distribution collapses to a single token, then $\text{SNR}^2(h) \rightarrow 0$ and detection becomes nearly impossible: the distribution converges so rapidly to a Dirac mass that small parameter perturbations cannot alter the outcome. If at least two logits are tied, $\text{SNR}^2(h)$ diverges and detectability is maximal: in the presence of ties, arbitrarily small parameter changes can force the model to select a single mode, making unimodal versus multimodal behavior easy to test. Moreover, under the conditions of Theorem 3.3, this divergence is obtained regardless of the model's weights, enabling a black-box approach.

A natural strategy for change detection is therefore to select x_{test} such that the logit distribution has at least two maximal entries. These inputs (termed **Border Inputs** or BIs) lie at the core of the change detection method presented next.

4. B3IT: Black-Box Border Input Tracking

Building upon Section 3, the B3IT method comprises two stages: *i*) an initialization stage whose goal is to identify border inputs (BIs) and their support, and *ii*) a detection stage whose goal is to detect a potential change of the target model compared to the initialization stage. As BIs leverage the low temperature phase transition, they exhibit high sensitivity to model changes: intuitively, if an input identified as a BI during initialization remains a BI during detection, then the model has likely not changed. We now describe both stages.

4.1. The B3IT Initialization Stage

The first step consists of finding BIs. While intuitively unlikely, in practice finding BIs turns out to be relatively easy on the majority of production models we tested, which allows B3IT to use a simple procedure: submit n random inputs m times at the lowest temperature T (possibly $T = 0$), and retain as BIs the \bar{n} inputs that produced more than one distinct output across their m draws.

More precisely, the phase transition phenomenon explored in Theorem 3.3 states that at $T \approx 0$ temperature, given an input x , only two situations can arise: either x is not a BI ($k = 1$), in which case it will always produce the same output token, or x is a BI ($k \geq 2$) and the output token is uniformly sampled among top tokens: a multinomial output distribution is observed.

The key parameter driving this stage is m , the number of samples collected per candidate BI x . A back-of-the-envelope analysis (see Section C) identifies $m = 3$ as an

optimal value if less than 75% of the candidates are BIs. This is the value we select in B3IT, which enables the discovery of BIs for less than 1,500 requests in a majority of production APIs (See Section 5.2).

Let x_{test} be an identified BI. To accurately estimate its initial distribution, it is sampled n_1 times.

4.2. The B3IT Detection Stage

The detection stage is to be triggered when a user wants to determine whether the target model has changed since the initialization stage. During detection, the temperature is set to its minimum (possibly $T = 0$) to operate in the optimal test regime.

In this regime, one can design simple tests with fully controlled nonasymptotic guarantees that are optimal for the practical use case considered here. As the output distribution concentrates on a (typically small) subset of tokens \mathcal{M} attaining the maximal log-probability, each with probability $1/k$, all remaining tokens receive zero probability. Consequently, the observed generation behavior can be modeled as sampling from a uniform distribution supported on an unknown finite subset of the token vocabulary.

Formally, we model the reference θ_0 and candidate θ_1 models by two unknown supports $S_1, S_2 \subset \Omega := \{1, \dots, d\}$ with corresponding output distributions $P = \text{Unif}(S_1)$ and $Q = \text{Unif}(S_2)$. We observe independent samples $X_1, \dots, X_{n_1} \sim P$ and $Y_1, \dots, Y_{n_2} \sim Q$, and aim to test whether the two models induce the same effective support, namely $H_0 : S_1 = S_2$ versus $H_1 : S_1 \neq S_2$.

In this setting, observing a token under one model that never appears under the other directly indicates a support mismatch. We therefore define the empirical supports $\hat{S}_1 := \{X_1, \dots, X_{n_1}\}$ and $\hat{S}_2 := \{Y_1, \dots, Y_{n_2}\}$, and the rejection event $\mathcal{R} := (\hat{S}_1 \setminus \hat{S}_2) \cup (\hat{S}_2 \setminus \hat{S}_1) \neq \emptyset$. In other words, B3IT rejects H_0 whenever \mathcal{R} occurs.

4.3. Analysis: Type-I and Type-II Errors

In this limit regime, we provide nonasymptotic guarantees for both Type-I and Type-II errors. We begin by controlling the Type-I error.

Theorem 4.1 (Type-I error). *Under $H_0 : S_1 = S_2$ with $|S| = k$, $\mathbb{P}_{H_0}(\mathcal{R}) \leq k \left(1 - \frac{1}{k}\right)^{n_1} + k \left(1 - \frac{1}{k}\right)^{n_2} \leq ke^{-n_1/k} + ke^{-n_2/k}$.*

Proof. See Section B.6. \square

We may also control the Type-II error as follows.

Theorem 4.2 (Type-II error). *Let $I := S_1 \cap S_2$, $k_1 := |S_1|$, $k_2 := |S_2|$ and set $p_1 := \frac{|I|}{k_1} \in [0, 1]$, $p_2 := \frac{|I|}{k_2} \in [0, 1]$.*

Under $H_1 : S_1 \neq S_2$, the probability of not rejecting satisfies $\mathbb{P}_{H_1}(\mathcal{R}^c) \leq p_1^{n_1} p_2^{n_2}$.

Proof. See Section B.7. \square

Experimental guidelines In typical zero-temperature LLM evaluations, the effective support of the reference model is small (often $k \in \{2, 3\}$), while the candidate model collapses to a single dominant token, i.e., $|S_1| = k$ and $|S_2| = 1 \subset S_1$ under H_1 .

In this practical alternative, Theorem 4.2 gives $\mathbb{P}_{H_1}(\mathcal{R}^c) \leq k^{-n_1}$, so the power depends only on the number of samples drawn from the reference model.

Under H_0 with $|S_1| = |S_2| = k$, false rejections occur only if at least one empirical support fails to observe all k tokens. By Theorem 4.1, $\mathbb{P}_{H_0}(\mathcal{R}) \leq ke^{-n_1/k} + ke^{-n_2/k}$. The parameter k therefore plays a central role, governing the tradeoff between Type-I and Type-II errors.

4.4. B3IT is Optimal for $k = 2$

The support-mismatch test based on \mathcal{R} is intentionally conservative: it rejects only when a token observed under one model is absent from the other empirical support. This choice yields simple nonasymptotic guarantees, but can be suboptimal when the effective support size k is large.

This limitation is immaterial in the zero-temperature regime we consider. Empirically, the effective support is typically very small (often $k \in \{2, 3\}$), and the dominant failure mode corresponds to a collapse of the candidate support to a singleton, i.e., $|S_1| = k$ while $|S_2| = 1 \subset S_1$.

Theorem 4.3 (Lower bound). *$H_0 : S_1 = S_2, |S_1| = 2$ vs $H_1 : |S_1| = 2, |S_2| = 1, S_2 \subset S_1$ with $n_1 = n_2 = n$. For any rejection region \mathcal{R} , $\mathbb{P}_{H_0}(\mathcal{R}) + \mathbb{P}_{H_1}(\mathcal{R}^c) \geq 2^{-(n+1)}$.*

Proof. See Section B.8. \square

This lower bound formalizes the unavoidable trade-off induced by sampling noise: no test can simultaneously achieve vanishing Type-I and Type-II errors, so reducing one necessarily increases the other.

Although its assumptions may appear restrictive, they capture the dominant regime observed in our experiments, where two top logits collapse to a single mode after the model θ_1 has been tampered with. Moreover, when combined with Theorem 4.1 and Theorem 4.2, this lower bound shows that the test introduced in this subsection is optimal up to a constant factor in this practical setting.

Takeaway. We present B3IT, a change detector that leverages BIs to implement a request-optimal change detection test. B3IT is very simple: the initialization stage identifies

one (or a handful of) BIs and samples their initial distribution. The detection step samples BIs again and compares the result with the initial distribution. Thanks to the low temperature, this test simply consists in comparing the support of uniform distributions. B3IT’s pseudo-code is provided in Algorithms 1 and 2.

5. Experimental Evaluation of B3IT

We validate B3IT both *in vitro* on a controlled benchmark, and *in vivo* on commercial LLM APIs. Our experiments address two questions: (1) can BIs be found efficiently in practice, and (2) how does B3IT compare to existing methods in accuracy and cost?

On the existence of BIs. In theory, logits lie in \mathbb{R} , so exact ties have probability zero. In practice, however, we observe many such ties. We attribute this to two factors: limited floating-point precision (causing rounding), and inference-time non-determinism (Chauvin et al., 2026; He & Lab, 2025).

5.1. In-Vitro Evaluation: TinyChange Benchmark

5.1.1. EXPERIMENTAL SETUP

We use the TinyChange benchmark (Chauvin et al., 2026), which generates controlled perturbations of open-weight LLMs, enabling systematic evaluation across varying change magnitudes.

Models. We evaluate on 9 instruction-tuned LLMs ranging from 0.5B to 9B parameters: Qwen2.5-0.5B, Gemma-3-1B, Phi-4-mini, Qwen2.5-7B, DeepSeek-R1-Distill-Qwen-7B, Mistral-7B, OLMo-2-1124-7B, Llama-3.1-8B, and Gemma-2-9B. The exact model IDs can be found in Section D.1.

Perturbation types. For each model, we generate a number of *variants*, created from the TinyChange difficulty scales with these parameters: (i) **Fine-tuning**: regular or LoRA (Hu et al., 2022), for 1 epoch with 1 to 4096 single-sample steps; (ii) **Unstructured pruning**: by magnitude or random selection, removing fractions from 2^{-20} to 1; (iii) **Parameter noise**: Gaussian perturbations with standard deviation $\sigma \in [2^{-30}, 1]$.

Baselines. We compare against two black-box methods, MMLU-ALG (Chauvin et al., 2026) and MET (Gao et al., 2025), and one grey-box method, LT (Chauvin et al., 2026), which requires access to log-probabilities.

Metrics. A change detection method should have a good classifier performance, and a low cost. For each method, we

therefore report (i) ROC AUC¹ averaged across all models and variants, and (ii) yearly cost of hourly monitoring at GPT-4.1 pricing.

Test statistic. The theory in Section 3 yields a binary support-mismatch test. To construct ROC curves, we need a threshold to vary. We therefore compute the total variation (TV) distance between reference and detection samples as a continuous statistic. For better performance, we also get samples from several prompts, averaging the per-prompt TV distance to obtain a test statistic.

5.1.2. INITIALIZATION STAGE

The goal of this stage is to identify BIs at minimal cost. We generate candidate prompts with minimal input length using each model’s tokenizer (see Section D.4), then sample each candidate $m = 3$ times at $T = 0$. We use synthetic noise similar to that of LT (Chauvin et al., 2026), by mixing our queries with simulated request traffic. A prompt is selected as a BI when it yields more than one unique output across the samples.

For comprehensive evaluation, we sample 20,000 prompts per model, collecting 1,000 reference samples per identified BI (though only 50 are used per test). We obtained 105 to 1,182 BIs depending on the model.

5.1.3. EXPERIMENTAL RESULTS

Hyperparameter selection. Figure 1 shows performance versus cost for various choices of prompt count and samples per prompt. Notably, increasing the number of prompts used can increase performance, holding the cost fixed: for instance, sampling 5 prompts 10 times outperforms sampling a single prompt 50 times. Several configurations achieve strong results; we select 5 prompts with 3 samples each, balancing accuracy and cost.

Comparison with baselines. Figure 2 presents performance versus cost. To ensure fair comparison, we sweep hyperparameters for baselines (including creating $T = 0$ variants of MMLU-ALG and MET) and fix 50 reference samples per prompt, varying only detection-time parameters.

B3IT substantially outperforms black-box methods, and approaches the grey-box LT baseline despite no access to log-probabilities. At operating point (\$2.2/year), B3IT achieves a ROC AUC of 0.9, whereas the next-best black-box method (MET at $T = 0$) reaches only 0.61. No black-box baseline reaches ROC AUC 0.9; the closest is MET at $T = 0$, which

¹Area under the ROC curve, which is the plot of the true positive rate (TPR) against the false positive rate (FPR) of a binary classifier, at each threshold setting

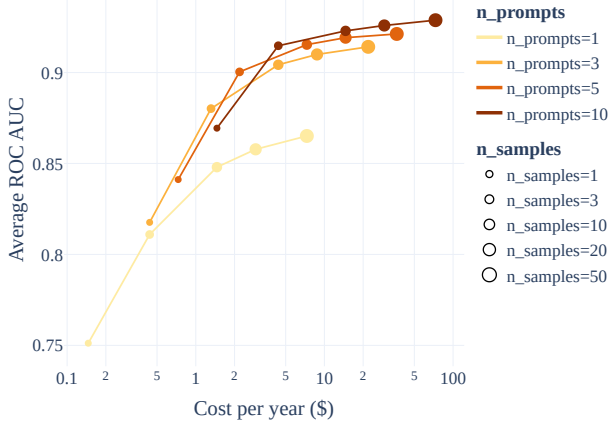


Figure 1. Performance increases with cost. We select 5 prompts and 3 samples/prompt for subsequent experiments.

requires \$67/year to reach 0.88.

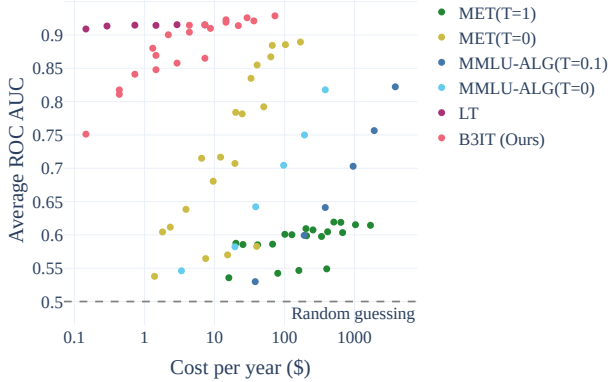


Figure 2. B3IT outperforms all black-box methods by a wide margin, and approaches the performance of the grey-box LT method.

Performance by change difficulty. Figure 3 shows detection performance on the fine-tuning difficulty scale. MMLU-ALG, and to a lesser extent MET, exhibit a low detection accuracy. B3IT and LT perform very well in detecting finetuned instances. As the number of fine-tuning steps decreases, the impact on model weights diminishes, increasing the detection difficulty. B3IT retains a 0.87 ROC-AUC for detecting the extreme single-step fine-tuning. Refer to Section D.8 for the performances facing other perturbations.

5.2. In-Vivo Evaluation: Commercial LLM APIs

5.2.1. ENDPOINT SELECTION

Starting from all endpoints listed on OpenRouter, we apply the following filters: (i) exclude endpoints costing above \$30 per million tokens (input + output), (ii) exclude free endpoints, which are often unreliable, and (iii) exclude endpoints where a single-letter input produces more than 10

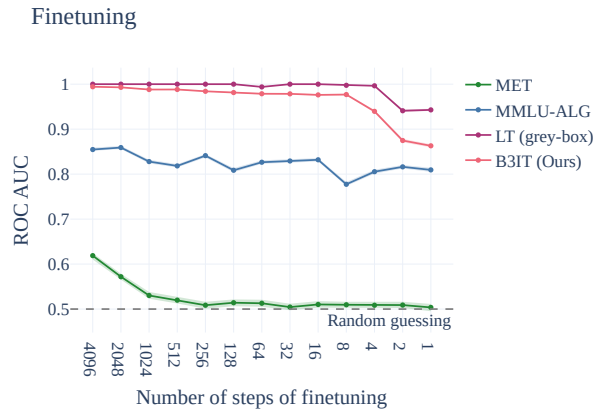


Figure 3. Detection performance on the TinyChange fine-tuning difficulty scale.

input tokens or more than 1 output token. This yields 373 candidate endpoints from 38 providers. We select 93, with at least one per provider, covering 64 unique models.

5.2.2. PREVALENCE OF BORDER INPUTS

Figure 4 reports the empirical CDF of requests required to find BIs across endpoints ($1,000$ inputs $\times 3$ queries each). At $T = 0$, 62% of endpoints yield at least one BI. Increasing the temperature to $T > 0$ raises this to about 80%, though at the cost of reduced BI quality (higher prevalence implies less selective detection).

For 18 of the endpoints, no BIs were found at any temperature. All of them systematically returned an empty string to all inputs. Two of them appeared to require at least 2 tokens of output to return a non-empty response, possibly due to a billed but non-rendered initial token; the other 16 were reasoning models, where reasoning couldn't be disabled and no output could be obtained with reasonably short output token limits. This constitutes a limitation of methods seeking to cheaply detect changes such as B3IT.

Finally, we observe an interesting behavior where many endpoints seem to behave differently at $T = 0$ than their limit as $T \rightarrow 0$ would indicate, which we hypothesize is due to hard-coded patterns at $T = 0$ (Anthropic, 2025).

5.2.3. CONTINUOUS MONITORING RESULTS

We keep the parameters of the in-vitro experiments: 5 prompts, 50 reference samples and 3 detection samples.

We therefore searched for 5 BIs at $T = 0$ (again, sampling each candidate $m = 3$ times) and found them in 54 endpoints. We sampled them 50 times to generate the reference distribution, then sampled each 3 times every 24h over a period of 23 days.

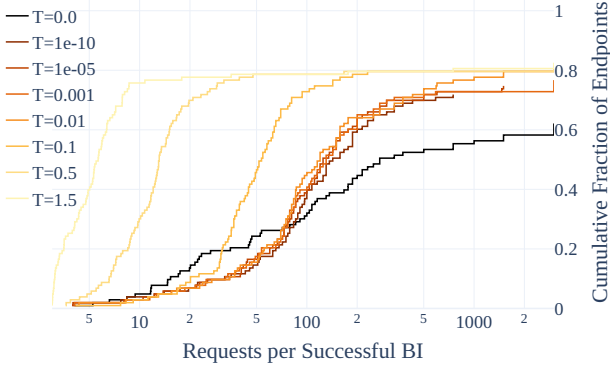


Figure 4. Empirical CDF of requests per BI across endpoints, for various temperatures.

At an average (input, output) endpoint cost of (\$0.38, \$1.2) / million tokens, the average cost of *hourly* monitoring would be \$0.52 per endpoint per year. At \$0.0045 per endpoint, the cost of the initialization stage is negligible compared to the ongoing detection cost.

We identified persistent changes where the mean TV remained below a threshold of 0.5 for at least 4 days, before crossing above for an equal period. Indeed, as suggested by our theoretical analysis, the token distribution on BIs quickly collapses to a single dominant mode under small perturbations; a TV = 0.5 marks the transition from a bimodal to a unimodal distribution. 8 endpoints were identified in this way (depicted on Figure 5). One of these is directly corroborated by Together AI’s public changelog, which on January 29 redirected Mistral-7B-Instruct-v0.3 to the entirely different Minstral-3-14B-Instruct-2512 (Together AI, 2026); the two DeepSeek-V3-0324 changes on Hyperbolic and Atlas Cloud may also relate to a January 23 Together changelog entry redirecting that model to DeepSeek-V3.1, suggesting a similar swap may have occurred across providers.

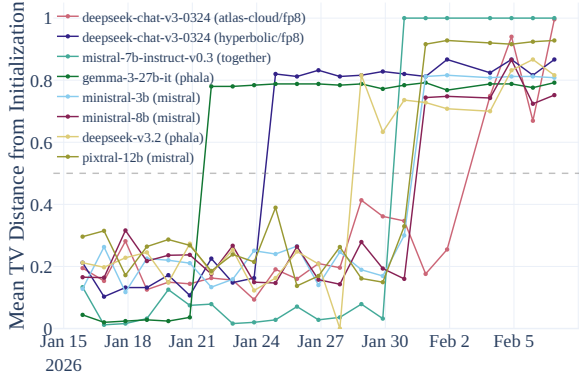


Figure 5. Detected changes on endpoints over 23 days.

6. Related Work

Change detection of models behind APIs. Tracking shifts in (non-LLM) ML APIs was introduced by (Chen et al., 2022), who found significant shifts in a third of the APIs they tested. For LLMs specifically, black-box methods include MET (Gao et al., 2025) (one of our baselines), which compared output distributions using a Maximum Mean Discrepancy test with a Hamming kernel. Daily-Bench (Phillips, 2025) attempted continuous benchmark-based monitoring of 5 LLM APIs using HELMLite (Liang et al., 2023), but was discontinued after 40 days due to substantial cost. On the white-box side (requiring access to reference model weights), ESF (Bai et al., 2025) selects sensitive inputs by analyzing penultimate-layer embeddings; TRAP (Gubri et al., 2024) optimizes adversarial suffixes via gradient-based search on a reference model; Token-DiFR (Karvonen et al., 2025) compares output tokens against a trusted reference conditioned on the same random seed, or at temperature 0. LT (Chauvin et al., 2026) operates in a grey-box setting, exploiting log probabilities for highly cost-effective monitoring. (Cai et al., 2025) re-implemented and compared several detection techniques.

Non-determinism in LLM inference. As change detection methods become increasingly sensitive, calibrating against hardware-induced noise becomes critical. (He & Lab, 2025) showed that run-to-run LLM non-determinism stems from varying batch sizes under server load, and proposed batch-invariant kernels as a fix. (Zhang et al., 2025) leveraged within-platform determinism and cross-platform non-determinism to fingerprint the hardware and software configuration of a given model, using a logprob-based method.

LLM fingerprinting. LLM fingerprinting is related to change detection, but aims to identify which model is being served, typically within a closed set, and methods often attempt to remain robust to small model variations. (Pasquini et al., 2025) introduced handcrafted queries paired with a classifier to match an LLM to a known model, explicitly seeking invariance to minor changes. (Sun et al., 2025) fine-tuned embedding models on LLM-generated texts to distinguish between a set of 5 models. (Chen et al., 2024) compared explicitly different ChatGPT versions across benchmarks, which can also be seen as coarse-grained fingerprinting. Change detection, by contrast, aims to trigger on *any* change, however small.

7. Conclusion

Change detection in LLMs behind APIs is becoming an important primitive for ensuring the reliability of downstream workflows. In this work, we established theoretical

foundations for black-box change detection with a single output token, revealing a phase transition at low temperature: border inputs (BIs), where multiple tokens are tied at the maximal logit, yield diverging signal-to-noise ratios, making even subtle parameter changes detectable. Building on this insight, we proposed B3IT, a practical method that discovers BIs through black-box sampling and monitors them at minimal cost. Our experiments validate B3IT on both controlled benchmarks and 93 commercial endpoints across 20 providers, demonstrating detection performance comparable to grey-box methods at 1/30th the cost of the best black-box alternatives. Future work could extend the theoretical framework beyond single-token observations to sequential multi-token settings, which might unlock even more sensitive and cost-efficient detection schemes.

8. Acknowledgments

We would like to thank Gersende Fort, Jean-Christophe Mourrat and Matthieu Jonckheere for their help at an early stage of this project.

Timothée Chauvin, Erwan Le Merrer, François Taïani and Gilles Trédan acknowledge the support of the French Agence Nationale de la Recherche (ANR), under grant ANR-24-CE23-7787 (project PACMAM).

This project was provided with computing (AI) and storage resources by GENCI at IDRIS thanks to the grant 2025-AD011016369 on the supercomputer Jean Zay's H100 partition.

This work was supported by the Cluster SequoIA Chair FANG funded by ANR, reference number ANR-23-IACL-0009.

References

Acharya, J., Das, H., Orlitsky, A., and Suresh, A. T. A unified maximum likelihood approach for estimating symmetric properties of discrete distributions. In *International Conference on Machine Learning (ICML)*, pp. 11–21, 2017a.

Acharya, J., Orlitsky, A., Suresh, A. T., and Tyagi, H. Estimating renyi entropy of discrete distributions. *IEEE Transactions on Information Theory*, 63(1):38–56, 2017b. doi: 10.1109/TIT.2016.2620435.

Acharya, J., Sun, Z., and Zhang, H. Differentially private testing of identity and closeness of discrete distributions. In *Advances in Neural Information Processing Systems (NeurIPS)*, volume 31. Curran Associates, Inc., 2018.

Acharya, J., Bhadane, S., Indyk, P., and Sun, Z. Estimating entropy of distributions in constant space. In *Advances in Neural Information Processing Systems (NeurIPS)*, volume 32. 2019.

Aliakbarpour, M., Indyk, P., Rubinfeld, R., and Silwal, S. Optimal algorithms for augmented testing of discrete distributions. In *Advances in Neural Information Processing Systems (NeurIPS)*, volume 37, pp. 11186–11227, 2024.

Anthropic. A postmortem of three recent issues. <https://www.anthropic.com/engineering/a-postmortem-of-three-recent-issues>, 2025. Accessed: 2026-01-01.

Babuschkin, I. <https://x.com/ibab/status/1893774017376485466>, 2025. Accessed: 2025-09-24.

Bai, X., Hu, P., Ma, X., Yu, L., Zhang, D., Zhang, Q., and Zhu, B. B. ESF: Efficient sensitive fingerprinting for black-box tamper detection of large language models. In *Findings of the Association for Computational Linguistics: ACL 2025*, pp. 10477–10494, July 2025.

Balakrishnan, S. and Wasserman, L. Hypothesis testing for densities and high-dimensional multinomials: Sharp local minimax rates. *The Annals of Statistics*, 47(4):1893–1927, 08 2019.

Barron, A. Uniformly powerful goodness of fit tests. *The Annals of Statistics*, 17, 03 1989.

Berrett, T. and Butucea, C. Locally private non-asymptotic testing of discrete distributions is faster using interactive mechanisms. In *Advances in Neural Information Processing Systems (NeurIPS)*, volume 33, pp. 3164–3173, 2020.

Cai, T. T., Ke, Z. T., and Turner, P. Testing high-dimensional multinomials with applications to text analysis. *Journal of the Royal Statistical Society Series B: Statistical Methodology*, 86(4):922–942, 02 2024.

Cai, W., Shi, T., Zhao, X., and Song, D. Are you getting what you pay for? auditing model substitution in llm apis. 2025. arXiv preprint arXiv:2504.04715.

Chauvin, T., Merrer, E. L., Taiani, F., and Tredan, G. Log probability tracking of LLM APIs. In *International Conference on Learning Representations (ICLR)*, 2026.

Chen, L., Zaharia, M., and Zou, J. How did the model change? efficiently assessing machine learning API shifts. In *International Conference on Learning Representations (ICLR)*, 2022.

Chen, L., Zaharia, M., and Zou, J. How Is ChatGPT’s Behavior Changing Over Time? *Harvard Data Science Review*, 6(2), mar 12 2024.

Cressie, N. and Read, T. R. Multinomial goodness-of-fit tests. *Journal of the Royal Statistical Society: Series B (Methodological)*, 46(3):440–464, 12 2018.

Gao, I., Liang, P., and Guestrin, C. Model equality testing: Which model is this API serving? In *International Conference on Learning Representations (ICLR)*, 2025.

Gubri, M., Ulmer, D., Lee, H., Yun, S., and Oh, S. J. TRAP: Targeted random adversarial prompt honeypot for black-box identification. In Ku, L.-W., Martins, A., and Srikanth, V. (eds.), *Findings of the Association for Computational Linguistics: ACL 2024*, pp. 11496–11517, August 2024.

He, H. and Lab, T. M. Defeating nondeterminism in llm inference. *Thinking Machines Lab: Connectionism*, 2025. doi: 10.64434/tml.20250910.

Hu, E. J., Shen, Y., Wallis, P., Allen-Zhu, Z., Li, Y., Wang, S., Wang, L., and Chen, W. Lora: Low-rank adaptation of large language models. In *International Conference on Learning Representations (ICLR)*, 2022.

Kairouz, P., Bonawitz, K., and Ramage, D. Discrete distribution estimation under local privacy. In *International Conference on Machine Learning (ICML)*, pp. 2436–2444. JMLR.org, 2016.

Karvonen, A., Reuter, D., Rinberg, R., Marks, L., Garriga- Alonso, A., and Warr, K. Diffr: Inference verification despite nondeterminism. 2025. arXiv preprint arXiv:2511.20621.

Kim, I. Multinomial goodness-of-fit based on u -statistics: High-dimensional asymptotic and minimax optimality. *Journal of Statistical Planning and Inference*, 205, 06 2019.

Lehmann, E. L. and Romano, J. P. *Testing statistical hypotheses*. Springer Texts in Statistics. Springer, New York, third edition, 2005.

Liang, P., Bommasani, R., Lee, T., Tsipras, D., Soylu, D., Yasunaga, M., Zhang, Y., Narayanan, D., Wu, Y., Kumar, A., Newman, B., Yuan, B., Yan, B., Zhang, C., Cosgrove, C., Manning, C. D., Re, C., Acosta-Navas, D., Hudson, D. A., Zelikman, E., Durmus, E., Ladhak, F., Rong, F., Ren, H., Yao, H., WANG, J., Santhanam, K., Orr, L., Zheng, L., Yuksekgonul, M., Suzgun, M., Kim, N., Guha, N., Chatterji, N. S., Khattab, O., Henderson, P., Huang, Q., Chi, R. A., Xie, S. M., Santurkar, S., Ganguli, S., Hashimoto, T., Icard, T., Zhang, T., Chaudhary, V., Wang, W., Li, X., Mai, Y., Zhang, Y., and Koreeda, Y. Holistic evaluation of language models. *Transactions on Machine Learning Research*, 2023.

Louati, S. Estimation of discrete distributions with high probability under χ^2 -divergence. 2025. arXiv preprint arXiv:2510.25400.

Neyman, J. and Pearson, E. S. On the problem of the most efficient tests of statistical hypotheses. *Philosophical Transactions of the Royal Society of London. Series A, Containing Papers of a Mathematical or Physical Character*, 231:289–337, 1933.

Ouvrard, J.-Y. *Probabilités 2*. Cassini, Paris:, 2è éd. edition, 2009. Index: pp. (553-557) Bibliogr. pp. (551-552).

Pasquini, D., Kornaropoulos, E. M., and Ateniese, G. Llmmap: fingerprinting for large language models. In *Proceedings of the 34th USENIX Conference on Security Symposium, SEC '25*. USENIX Association, 2025.

Phillips, J. daily-bench. <https://github.com/jacobphillips99/daily-bench>, 2025.

Sun, M., Yin, Y., Xu, Z., Kolter, J. Z., and Liu, Z. Idiosyncrasies in large language models. In *International Conference on Machine Learning (ICML)*, 2025.

Together AI. Changelog, 2026. URL <https://docs.together.ai/docs/changelog>. Accessed: 2026-02-09.

Tsybakov, A. B. *Introduction to Nonparametric Estimation*. Springer series in statistics. Springer, 2009.

van der Vaart, A. W. *Asymptotic Statistics*. Cambridge University Press, 1998.

xAI. <https://x.com/grok/status/1943916977481036128>, 2025a. Accessed: 2025-09-24.

xAI. <https://x.com/xai/status/1923183620606619649>, 2025b. Accessed: 2025-09-24.

Zhang, C., Foerster, H., Mullins, R. D., Zhao, Y., and Shumailov, I. Hardware and software platform inference. In *International Conference on Machine Learning (ICML)*, 2025.

Zheng, Z., Ning, K., Zhong, Q., Chen, J., Chen, W., Guo, L., Wang, W., and Wang, Y. Towards an understanding of large language models in software engineering tasks. *Empirical Software Engineering*, 30(2):50, 2025.

A. Notations

\Rightarrow denotes convergence in distribution, and more broadly the weak convergence when applied to measures of probability. For two sequences of random vectors (U_n) and (V_n) , we write $U_n = o_{\mathbb{P}}(V_n)$ (resp. $U_n = O_{\mathbb{P}}(V_n)$) if there exists a sequence of random vectors (W_n) such that $U_n = W_n V_n$ and (W_n) converges in \mathbb{P} -probability to 0 (resp. is uniformly tight). If the base probability measure depends on n , we say that (W_n) converges in \mathbb{P}_n -probability to 0 if $\forall \epsilon > 0$, $\mathbb{P}_n(\|W_n\| > \epsilon) \rightarrow 0$. Deterministic Landau notations have their usual meaning. Unless stated otherwise, $\|\cdot\|$ denotes the Euclidean norm, and for a matrix M , $\|M\|_{\text{op}}$ and $\|M\|_{\text{F}}$ denote its operator and Frobenius norms. For a symmetric matrix $A \succeq 0$, we write $\|x\|_A^2 := x^T A x$. We use $\text{tr}(\cdot)$ and $\det(\cdot)$ for trace and determinant. The indicator function is denoted by $1\{\cdot\}$, and I_d denotes the $d \times d$ identity matrix. The Kronecker product is denoted by \otimes , and $\text{vec}(\cdot)$ denotes vectorization (column-stacking). We write $\mathcal{N}(\mu, \Sigma)$ for the Gaussian distribution with mean μ and covariance Σ . For probability measures P and Q on a common measurable space, $\text{TV}(P, Q)$ denotes their total variation distance. The natural logarithm is denoted by \log . i may refer to the canonical complex number that solves " $i = \sqrt{-1}$ " which should be clearly identifiable in context. \mathbb{S}^{q-1} is the unit sphere in \mathbb{R}^q . For a set S , $\text{Unif}(S)$ denotes the uniform distribution on S . The rest of the notations are either standard or introduced within text.

B. Proofs

B.1. Log-likelihood ratio in the LAN regime

We note $Z_n := \sqrt{n}(T_n - \mathbf{p}_0)$ and $\mathbf{d} := Jh$.

We note $\mathbf{p}_0 = (p_{0,1}, \dots, p_{0,d-1})$ and $p_{0,d} := 1 - \sum_{j=1}^{d-1} p_{0,j} > 0$. Likewise, we note $\mathbf{p}_n = (p_{n,1}, \dots, p_{n,d-1})$ and $p_{n,d} := 1 - \sum_{j=1}^{d-1} p_{n,j} > 0$.

We write the multinomial counts $N_j := \sum_{i=1}^n \mathbf{1}\{Y_i = j\}$ for $j = 1, \dots, d$, $\hat{p}_j := N_j/n$ for $j \leq d-1$ and $\hat{p}_d := 1 - \sum_{j=1}^{d-1} \hat{p}_j = N_d/n$.

The log-likelihood ratio is (\mathbf{p}_n numerator and \mathbf{p}_0 denominator)

$$\begin{aligned} \log \Lambda_n &= \sum_{j=1}^d N_j \log \left(\frac{p_{n,j}}{p_{0,j}} \right) \\ &= n \sum_{j=1}^d \hat{p}_j \log \left(\frac{p_{n,j}}{p_{0,j}} \right). \end{aligned} \tag{3}$$

We define $\Delta_n := \mathbf{p}_n - \mathbf{p}_0 \in \mathbb{R}^{d-1}$ and $\Delta_{n,d} := p_{n,d} - p_{0,d} = -\mathbf{1}^T \Delta_n$. By assumption,

$$\Delta_n = \frac{s}{\sqrt{n}} \mathbf{d} + r_n, \tag{4}$$

where $\sqrt{n}\|r_n\| \rightarrow 0$.

Let us start with the following Taylor expansions : For $j \leq d-1$,

$$\log \left(\frac{p_{n,j}}{p_{0,j}} \right) = \frac{\Delta_{n,j}}{p_{0,j}} - \frac{1}{2} \frac{\Delta_{n,j}^2}{p_{0,j}^2} + R_{n,j}, \quad R_{n,j} = O\left(\frac{|\Delta_{n,j}|^3}{p_{0,j}^3}\right), \tag{5}$$

and similarly for the d -th coordinate,

$$\log \left(\frac{p_{n,d}}{p_{0,d}} \right) = \frac{\Delta_{n,d}}{p_{0,d}} - \frac{1}{2} \frac{\Delta_{n,d}^2}{p_{0,d}^2} + R_{n,d}, \quad R_{n,d} = O\left(\frac{|\Delta_{n,d}|^3}{p_{0,d}^3}\right). \tag{6}$$

Since \mathbf{p}_0 is interior, all $p_{0,j}$'s are bounded away from 0, hence $\sum_{j=1}^d |R_{n,j}| = O(\|\Delta_n\|^3)$. Multiplying by n gives

$$\begin{aligned}
 n \sum_{j=1}^d \hat{p}_j R_{n,j} &\stackrel{\text{Holder}}{\leq} n \left(\max_j \hat{p}_j \right) \left(\sum_{j=1}^d |R_{n,j}| \right) \\
 &\stackrel{\text{a.s.}}{\leq} n O(\|\Delta_n\|^3) \\
 &\stackrel{\text{a.s.}}{\leq} O(n \cdot n^{-3/2}) \\
 &\stackrel{\text{a.s.}}{\leq} O(n^{-1/2}) \\
 &\leq o_{\mathbb{P}_{\mathbf{p}_0, \mathbf{p}_n}}(1),
 \end{aligned} \tag{7}$$

because $\|\Delta_n\| = O(1/\sqrt{n})$ and because the \hat{p}_j 's are almost surely in $[0, 1]$.

Plugging the expansions into (3) yields

$$\log \Lambda_n = n \sum_{j=1}^d \hat{p}_j \frac{\Delta_{n,j}}{p_{0,j}} - \frac{n}{2} \sum_{j=1}^d \hat{p}_j \frac{\Delta_{n,j}^2}{p_{0,j}^2} + o_{\mathbb{P}_{\mathbf{p}_0, \mathbf{p}_n}}(1). \tag{8}$$

First-order term. We decompose $\hat{p}_j = p_{0,j} + (\hat{p}_j - p_{0,j})$. It follows that

$$n \sum_{j=1}^d \hat{p}_j \frac{\Delta_{n,j}}{p_{0,j}} = n \sum_{j=1}^d \Delta_{n,j} + n \sum_{j=1}^d (\hat{p}_j - p_{0,j}) \frac{\Delta_{n,j}}{p_{0,j}}. \tag{9}$$

The first sum is $n \sum_{j=1}^d \Delta_{n,j} = 0$ because both \mathbf{p}_n and \mathbf{p}_0 sum to 1.

For the second sum, we write it in reduced coordinates: for $j \leq d-1$, $\hat{p}_j - p_{0,j} = Z_{n,j}/\sqrt{n}$, and for $j = d$, $\hat{p}_d - p_{0,d} = -(\mathbf{1}^T Z_n)/\sqrt{n}$. Also $\Delta_{n,d} = -(\mathbf{1}^T \Delta_n)$. Hence

$$n \sum_{j=1}^d (\hat{p}_j - p_{0,j}) \frac{\Delta_{n,j}}{p_{0,j}} = \sqrt{n} \left(\sum_{j=1}^{d-1} Z_{n,j} \frac{\Delta_{n,j}}{p_{0,j}} + (\mathbf{1}^T Z_n) \frac{\mathbf{1}^T \Delta_n}{p_{0,d}} \right). \tag{10}$$

Using $\Delta_n = \frac{s}{\sqrt{n}} \mathbf{d} + r_n$ and $\sqrt{n} \|r_n\| \rightarrow 0$, this becomes

$$n \sum_{j=1}^d \hat{p}_j \frac{\Delta_{n,j}}{p_{0,j}} = s \left(\sum_{j=1}^{d-1} Z_{n,j} \frac{d_j}{p_{0,j}} + (\mathbf{1}^T Z_n) \frac{\mathbf{1}^T \mathbf{d}}{p_{0,d}} \right) + o(1). \tag{11}$$

Second-order term. First, by the law of large numbers, under H_0 we have $\hat{p}_j \rightarrow p_{0,j}$ in probability.

Then, under H_1 , Hoeffding's inequality (see Lemma A.4 in (Tsybakov, 2009)) ensures that

$$\hat{p}_j - p_{0,j} \rightarrow 0 \tag{12}$$

in \mathbf{p}_n probability, and since $p_{n,j} \rightarrow p_{0,j}$ deterministically,

$$\hat{p}_j - p_{0,j} \rightarrow 0 \tag{13}$$

in probability.

In any case, $\hat{p}_j - p_{0,j} = o_{\mathbb{P}_{\mathbf{p}_0, \mathbf{p}_n}}(1)$.

So, since $\Delta_{n,j}^2 = O(1/n)$,

$$\begin{aligned}
 \frac{n}{2} \sum_{j=1}^d \hat{p}_j \frac{\Delta_{n,j}^2}{p_{0,j}^2} &= \frac{n}{2} \sum_{j=1}^d p_{0,j} \frac{\Delta_{n,j}^2}{p_{0,j}^2} + o_{\mathbb{P}_{H_0, H_1}}(1) \\
 &= \frac{n}{2} \sum_{j=1}^d \frac{\Delta_{n,j}^2}{p_{0,j}} + o_{\mathbb{P}_{H_0, H_1}}(1) \\
 &= \frac{s^2}{2} \left(\sum_{j=1}^{d-1} \frac{d_j^2}{p_{0,j}} + \frac{(\mathbf{1}^T \mathbf{d})^2}{p_{0,d}} \right) + o_{\mathbb{P}_{\mathbf{p}_0, \mathbf{p}_n}}(1).
 \end{aligned} \tag{14}$$

Conclusion of the proof. We have that

$$F^{-1}(\mathbf{p}_0) = \text{diag}(\mathbf{p}_0)^{-1} + \frac{1}{p_{0,d}} \mathbf{1} \mathbf{1}^T. \tag{15}$$

Therefore

$$\mathbf{d}^T F^{-1}(\mathbf{p}_0) Z_n = \sum_{j=1}^{d-1} Z_{n,j} \frac{d_j}{p_{0,j}} + (\mathbf{1}^T Z_n) \frac{\mathbf{1}^T \mathbf{d}}{p_{0,d}}, \tag{16}$$

and

$$\mathbf{d}^T F^{-1}(\mathbf{p}_0) \mathbf{d} = \sum_{j=1}^{d-1} \frac{d_j^2}{p_{0,j}} + \frac{(\mathbf{1}^T \mathbf{d})^2}{p_{0,d}}. \tag{17}$$

Combining (8), (11), (14) gives

$$\log \Lambda_n = s \mathbf{d}^T F^{-1}(\mathbf{p}_0) Z_n - \frac{s^2}{2} \mathbf{d}^T F^{-1}(\mathbf{p}_0) \mathbf{d} + o_{\mathbb{P}_{\mathbf{p}_0, \mathbf{p}_n}}(1), \tag{18}$$

which concludes the proof.

B.2. Proof of Theorem 3.1

By the Neyman-Pearson lemma (see theorem Theorem 3.2.1 in (Lehmann & Romano, 2005)), for a fixed $\alpha \in (0, 1)$, the most powerful test of level α (which exists) to test $H_0 : \mathbf{p}_0$ vs $H_1 : \mathbf{p}_n$ has exactly Type-I error α and is of the form

$$\phi = \begin{cases} 1 & \text{if } \log \Lambda_n > a_n \\ c_n & \text{if } \log \Lambda_n = a_n \\ 0 & \text{if } \log \Lambda_n < a_n \end{cases} \tag{19}$$

where $c_n \in [0, 1]$, $a_n \in \mathbb{R}$ satisfy $\mathbb{E}_{\mathbf{p}_0}(\phi) = \alpha$.

Under \mathbf{p}_0 , we have $Z_n \Rightarrow \mathcal{N}(0, F(\mathbf{p}_0))$ by the central limit theorem, hence Equation (18), Slutsky's lemma and the continuous mapping theorem (see (van der Vaart, 1998)) give

$$\log \Lambda_n \Rightarrow \mathcal{N}\left(-\frac{s^2}{2} h^T J^T F(\mathbf{p}_0)^{-1} J h, s^2 h^T J^T F(\mathbf{p}_0)^{-1} J h\right). \tag{20}$$

We may expand $\mathbb{E}_{\mathbf{p}_0}(\phi)$ as

$$\mathbb{E}_{\mathbf{p}_0}(\phi) = c_n \mathbb{P}_{\mathbf{p}_0}(\log \Lambda_n = a_n) + \mathbb{P}_{\mathbf{p}_0}(\log \Lambda_n > a_n). \tag{21}$$

Let us first prove that (a_n) converges to a finite limit. For the sake of contradiction, let us assume that (a_n) is unbounded. We extract a subsequence (b_n) that diverges (here we suppose that $b_n \rightarrow \infty$, the other case being treated in the same fashion). Without loss of generality, $\forall n, b_n > 0$. Then for every, $K > 0$, there exists a N such that for every $n \geq N$, $b_n > K$. Thus for every $n \geq N$,

$$\mathbb{E}_{\mathbf{p}_0}(\phi) \leq \mathbb{P}_{\mathbf{p}_0}(\log \Lambda_n \geq K), \quad (22)$$

and we know by the portmanteau lemma (2.2 in (van der Vaart, 1998)) that

$$\mathbb{P}_{\mathbf{p}_0}(\log \Lambda_n \geq K) \rightarrow \mathbb{P}\left(N\left(-\frac{s^2}{2}h^T J^T F(\mathbf{p}_0)^{-1} J h, s^2 h^T J^T F(\mathbf{p}_0)^{-1} J h\right) \geq K\right), \quad (23)$$

with the right hand side that tends to 0 when K tends to infinity. This contradicts the fact that all the tests are Type-I error α , and thus (a_n) is bounded.

We now show that (a_n) has a unique adherence point. Let a_∞ be an adherence point of (a_n) . Up to an extraction, we have $a_n \rightarrow a_\infty$.

We then have, by the portmanteau lemma

$$\mathbb{P}_{\mathbf{p}_0}(\log \Lambda_n > a_n) \rightarrow \mathbb{P}\left(N\left(-\frac{s^2}{2}h^T J^T F(\mathbf{p}_0)^{-1} J h, s^2 h^T J^T F(\mathbf{p}_0)^{-1} J h\right) > a_\infty\right). \quad (24)$$

Let (α, β) be an open interval containing a_∞ . Since $a_n \rightarrow a_\infty$, $a_n \in (\alpha, \beta)$ for n big enough. Thus for n big enough,

$$\mathbb{P}_{\mathbf{p}_0}(\log \Lambda_n = a_n) \leq \mathbb{P}_{\mathbf{p}_0}(\log \Lambda_n \in (\alpha, \beta)) \rightarrow \mathbb{P}\left(N\left(-\frac{s^2}{2}h^T J^T F(\mathbf{p}_0)^{-1} J h, s^2 h^T J^T F(\mathbf{p}_0)^{-1} J h\right) \in (\alpha, \beta)\right) \quad (25)$$

by the portmanteau lemma. Since this holds for any neighborhood (α, β) of a_∞ , $\mathbb{P}_{\mathbf{p}_0}(\log \Lambda_n = a_n) \rightarrow 0$. Since we know that all the tests have same level, there can only be one such a_∞

So (a_n) is bounded and has a unique adherence point, it thus converges. Let us note a_∞ this limit.

The last two equations also allow to calibrate a_∞ . Indeed since we know that the tests are of level α , $a_\infty = -\frac{s^2}{2}h^T J^T F(\mathbf{p}_0)^{-1} J h + \sqrt{s^2 h^T J^T F(\mathbf{p}_0)^{-1} J h} Q_\alpha$ where Q_α is the quantile of order $1 - \alpha$ of $\mathcal{N}(0, 1)$.

Let us look at the asymptotic Type-II error of this sequence of optimal tests. We may expand $\mathbb{E}_{\mathbf{p}_1}(\phi)$ as

$$\begin{aligned} 1 - \mathbb{E}_{\mathbf{p}_1}(\phi) &= 1 - c_n \mathbb{P}_{\mathbf{p}_1}(\log \Lambda_n = a_n) - \mathbb{P}_{\mathbf{p}_1}(\log \Lambda_n > a_n) \\ &= \mathbb{P}_{\mathbf{p}_1}(\log \Lambda_n \leq a_n) - c_n \mathbb{P}_{\mathbf{p}_1}(\log \Lambda_n = a_n). \end{aligned} \quad (26)$$

Recall the exact LAN expansion from Section B.1,

$$\log \Lambda_n = s \mathbf{d}^T F(\mathbf{p}_0)^{-1} Z_n - \frac{s^2}{2} \mathbf{d}^T F(\mathbf{p}_0)^{-1} \mathbf{d} + o_{\mathbb{P}_{\mathbf{p}_1}}(1). \quad (27)$$

Under H_1 we further decompose

$$Z_n = \sqrt{n}(T_n - \mathbf{p}_n) + \sqrt{n}(\mathbf{p}_n - \mathbf{p}_0). \quad (28)$$

By assumption, $\sqrt{n}(\mathbf{p}_n - \mathbf{p}_0) = s \mathbf{d} + o(1)$ deterministically. It remains to study $\underbrace{\sqrt{n}(T_n - \mathbf{p}_n)}_{=: Z'_n}$ under \mathbb{P}_{H_1} .

Here we would like to apply a central limit theorem to Z'_n and say that it is asymptotically Gaussian. However, the fact that the base probability measure changes with n is a problem that prevents the direct use of that result. We instead study this term by studying the Fourier transform of its probability measure directly and prove a CLT-like result that allows concluding the proof.

Fix $t \in \mathbb{R}^{d-1}$ and consider the characteristic function

$$\varphi_n(t) := \mathbb{E}_{\mathbf{p}_n} \left(e^{it^T Z'_n} \right) = \left(\mathbb{E}_{\mathbf{p}_n} \left(e^{it^T X_{n,1} \sqrt{n}} \right) \right)^n. \quad (29)$$

where $X_{n,1}$ is the one-hot encoding of the first categorical variable minus \mathbf{p}_n . Note that in the previous equation, we used the independence to transform a sum of random variables into a product of characteristic functions.

We need to control the Taylor development of this. Let $f(u) := e^{iu}$. By Taylor's theorem with integral remainder at order 2,

$$f(u) = f(0) + f'(0)u + \frac{1}{2}f''(0)u^2 + R_3(u), \quad R_3(u) = \int_0^u \frac{(u-s)^2}{2} f^{(3)}(s)ds. \quad (30)$$

Here

$$f'(u) = ie^{iu}, \quad f''(u) = -e^{iu}, \quad f^{(3)}(u) = -ie^{iu}. \quad (31)$$

Hence the remainder is exactly

$$R_3(u) = \int_0^u \frac{(u-s)^2}{2} (-i)e^{is} ds = -\frac{i}{2} \int_0^u (u-s)^2 e^{is} ds. \quad (32)$$

$$e^{iu} = 1 + iu - \frac{u^2}{2} - \frac{i}{2} \int_0^u (u-s)^2 e^{is} ds. \quad (33)$$

Thus,

$$|R_3(u)| \leq \frac{1}{2} \int_0^{|u|} (|u|-s)^2 ds = \frac{1}{2} \frac{|u|^3}{3} = \frac{|u|^3}{6}. \quad (34)$$

Applying it with $u = t^T X_{n,1} / \sqrt{n}$ yields

$$\mathbb{E}_{\mathbf{p}_n} \left(e^{it^T X_{n,1} / \sqrt{n}} \right) = 1 - \frac{1}{2n} t^T \mathbb{E}_{\mathbf{p}_n} (X_{n,1} X_{n,1}^T) t + R_n(t), \quad (35)$$

where the linear term vanishes because $\mathbb{E}_{\mathbf{p}_n}(X_{n,1}) = 0$, and where

$$|R_n(t)| \leq \mathbb{E}_{\mathbf{p}_n} \left(\left| e^{it^T X_{n,1} / \sqrt{n}} - 1 - \frac{i}{\sqrt{n}} t^T X_{n,1} + \frac{1}{2n} (t^T X_{n,1})^2 \right| \right) \lesssim \frac{\|t\|^3}{n^{3/2}}, \quad (36)$$

where we used the Taylor remainder bound for e^{ix} and the Hölder bound $|t^T X_{n,1}| \leq \|t\|_1$.

Hence

$$\log \varphi_n(t) = n \log \left(1 - \frac{1}{2n} t^T F(\mathbf{p}_n) t + R_n(t) \right) = -\frac{1}{2} t^T F(\mathbf{p}_n) t + o(1), \quad (37)$$

because $nR_n(t) = O(n^{-1/2}) \rightarrow 0$ for fixed t . Since $\mathbf{p}_n \rightarrow \mathbf{p}_0$ and $F(\cdot)$ is continuous on the interior, $F(\mathbf{p}_n) \rightarrow F(\mathbf{p}_0)$, so

$$\log \varphi_n(t) \rightarrow -\frac{1}{2} t^T F(\mathbf{p}_0) t, \quad (38)$$

which gives

$$\varphi_n(t) \rightarrow \exp \left(-\frac{1}{2} t^T F(\mathbf{p}_0) t \right). \quad (39)$$

Hence, if we note $\mu'_n := Z'_n \# \mathbf{p}_n$ the pushforward of \mathbf{p}_n by Z'_n , Lévi's continuity theorem for measures (see (Ouvrard, 2009) theorem 14.8) ensures than μ'_n weakly converges to the centered Gaussian probability measure with covariance matrix $F(\mathbf{p}_0)$.

Since

$$\log \Lambda_n = s \mathbf{d}^T F(\mathbf{p}_0)^{-1} Z_n - \frac{s^2}{2} \mathbf{d}^T F(\mathbf{p}_0)^{-1} \mathbf{d} + o_{\mathbb{P}_{\mathbf{p}_n}}(1), \quad (40)$$

we can write for any fixed $t \in \mathbb{R}$

$$\begin{aligned} \mathbb{E}_{\mathbf{p}_n} \left(e^{it \log \Lambda_n} \right) &= \mathbb{E}_{\mathbf{p}_n} \left(e^{it \left(s \mathbf{d}^T F(\mathbf{p}_0)^{-1} Z_n - \frac{s^2}{2} \mathbf{d}^T F(\mathbf{p}_0)^{-1} \mathbf{d} + o_{\mathbb{P}_{\mathbf{p}_n}}(1) \right)} \right) \\ &= \mathbb{E}_{\mathbf{p}_n} \left(e^{it \left(s \mathbf{d}^T F(\mathbf{p}_0)^{-1} Z_n - \frac{s^2}{2} \mathbf{d}^T F(\mathbf{p}_0)^{-1} \mathbf{d} + o_{\mathbb{P}_{\mathbf{p}_n}}(1) \right)} \right) \\ &= \mathbb{E}_{\mathbf{p}_n} \left(e^{it \left(s \mathbf{d}^T F(\mathbf{p}_0)^{-1} (Z'_n + s \mathbf{d} + o(1)) - \frac{s^2}{2} \mathbf{d}^T F(\mathbf{p}_0)^{-1} \mathbf{d} + o_{\mathbb{P}_{\mathbf{p}_n}}(1) \right)} \right) \\ &= \mathbb{E}_{\mathbf{p}_n} \left(e^{it \left(s \mathbf{d}^T F(\mathbf{p}_0)^{-1} (Z'_n + s \mathbf{d}) - \frac{s^2}{2} \mathbf{d}^T F(\mathbf{p}_0)^{-1} \mathbf{d} + o_{\mathbb{P}_{\mathbf{p}_n}}(1) \right)} \right) \end{aligned} \quad (41)$$

where the deterministic $o(1)$ was included in the o in probability.

Let us fix $\delta > 0$ and denote by R the random variable referred to as $o_{\mathbb{P}_{\mathbf{p}_1}}(1)$,

$$\begin{aligned}\mathbb{E}_{\mathbf{p}_n}(e^{it \log \Lambda_n}) &= \mathbb{E}_{\mathbf{p}_n}\left(e^{it\left(s\mathbf{d}^T F(\mathbf{p}_0)^{-1}(Z'_n+sd)-\frac{s^2}{2}\mathbf{d}^T F(\mathbf{p}_0)^{-1}\mathbf{d}+R\right)}(\mathbf{1}\{|R|>\delta\}+\mathbf{1}\{|R|\leq\delta\})\right) \\ &= \mathbb{E}_{\mathbf{p}_n}\left(e^{it\left(s\mathbf{d}^T F(\mathbf{p}_0)^{-1}(Z'_n+sd)-\frac{s^2}{2}\mathbf{d}^T F(\mathbf{p}_0)^{-1}\mathbf{d}+R\right)}\mathbf{1}\{|R|>\delta\}\right) \\ &\quad + \mathbb{E}_{\mathbf{p}_n}\left(e^{it\left(s\mathbf{d}^T F(\mathbf{p}_0)^{-1}(Z'_n+sd)-\frac{s^2}{2}\mathbf{d}^T F(\mathbf{p}_0)^{-1}\mathbf{d}+R\right)}\mathbf{1}\{|R|\leq\delta\}\right)\end{aligned}\quad (42)$$

Furthermore,

$$\begin{aligned}|\mathbb{E}_{\mathbf{p}_n}\left(e^{it\left(s\mathbf{d}^T F(\mathbf{p}_0)^{-1}(Z'_n+sd)-\frac{s^2}{2}\mathbf{d}^T F(\mathbf{p}_0)^{-1}\mathbf{d}+R\right)}\mathbf{1}\{|R|>\delta\}\right)| \\ \leq \mathbb{E}_{\mathbf{p}_n}\left(|e^{it\left(s\mathbf{d}^T F(\mathbf{p}_0)^{-1}(Z'_n+sd)-\frac{s^2}{2}\mathbf{d}^T F(\mathbf{p}_0)^{-1}\mathbf{d}+R\right)}|\mathbf{1}\{|R|>\delta\}\right) \\ \leq \mathbb{E}_{\mathbf{p}_n}(\mathbf{1}\{|R|>\delta\}) \\ \rightarrow 0\end{aligned}\quad (43)$$

since $R = o_{\mathbb{P}_{\mathbf{p}_1}}(1)$.

Furthermore,

$$\mathbb{E}_{\mathbf{p}_n}\left(\underbrace{e^{it\left(s\mathbf{d}^T F(\mathbf{p}_0)^{-1}(Z'_n+sd)-\frac{s^2}{2}\mathbf{d}^T F(\mathbf{p}_0)^{-1}\mathbf{d}+R\right)}\mathbf{1}\{|R|\leq\delta\}}_{\in B(e^{it\left(s\mathbf{d}^T F(\mathbf{p}_0)^{-1}(Z'_n+sd)-\frac{s^2}{2}\mathbf{d}^T F(\mathbf{p}_0)^{-1}\mathbf{d}\right)},\delta')}\right)\quad (44)$$

where $B(c, r)$ is the ball in \mathbb{C} centered at c and of radius r and where $\delta' = \sup_{-\delta \leq r' \leq \delta} \left| e^{it\left(s\mathbf{d}^T F(\mathbf{p}_0)^{-1}(Z'_n+sd)-\frac{s^2}{2}\mathbf{d}^T F(\mathbf{p}_0)^{-1}\mathbf{d}+r'\right)} - e^{it\left(s\mathbf{d}^T F(\mathbf{p}_0)^{-1}(Z'_n+sd)-\frac{s^2}{2}\mathbf{d}^T F(\mathbf{p}_0)^{-1}\mathbf{d}\right)} \right|$.

Thus, for any n big enough, by continuity,

$$\mathbb{E}_{\mathbf{p}_n}(e^{it \log \Lambda_n}) \in B\left(\mathbb{E}_{\mathbf{p}_n}\left(e^{it\left(s\mathbf{d}^T F(\mathbf{p}_0)^{-1}(Z'_n+sd)-\frac{s^2}{2}\mathbf{d}^T F(\mathbf{p}_0)^{-1}\mathbf{d}\right)}\right), r(\delta)\right) \quad (45)$$

where r is non-negative and tends to 0 as δ tends to 0.

Thus, since this holds true for any δ , showing the convergence of $\mathbb{E}_{\mathbf{p}_n}\left(e^{it\left(s\mathbf{d}^T F(\mathbf{p}_0)^{-1}(Z'_n+sd)-\frac{s^2}{2}\mathbf{d}^T F(\mathbf{p}_0)^{-1}\mathbf{d}\right)}\right)$ would be sufficient to show the convergence of $\mathbb{E}_{\mathbf{p}_n}(e^{it \log \Lambda_n})$ to the same limit as it would be a bounded sequence with only one adherence point.

Furthermore, by the weak convergence of μ'_n , we immediately have (see (Ouvrard, 2009) Proposition 14.5) that $\mathbb{E}_{\mathbf{p}_n}\left(e^{it\left(s\mathbf{d}^T F(\mathbf{p}_0)^{-1}(Z'_n+sd)-\frac{s^2}{2}\mathbf{d}^T F(\mathbf{p}_0)^{-1}\mathbf{d}\right)}\right)$ pointwise converges to the characteristic function of a Gaussian of mean $\frac{s^2}{2}h^T J^T F(\mathbf{p}_0)^{-1}Jh$ and of covariance matrix $s^2h^T J^T F(\mathbf{p}_0)^{-1}Jh$.

Hence, if we note $\mu_n := \log \Lambda_n \# \mathbf{p}_n$ the pushforward of \mathbf{p}_n by $\log \Lambda_n$, Lévi's continuity theorem for measures again ensures that μ_n weakly converges to a Gaussian probability measure with mean $\frac{s^2}{2}h^T J^T F(\mathbf{p}_0)^{-1}Jh$ and of covariance matrix $s^2h^T J^T F(\mathbf{p}_0)^{-1}Jh$.

This gives that

$$\begin{aligned}\mathbb{P}_{\mathbf{p}_n}(\log \Lambda_n \leq a_n) &= \mu_n((-\infty, a_\infty]) + (\mu_n((-\infty, a_n]) - \mu_n((-\infty, a_\infty])) \\ &\rightarrow \mathbb{P}\left(\mathcal{N}\left(\frac{s^2}{2}h^T J^T F(\mathbf{p}_0)^{-1}Jh, s^2h^T J^T F(\mathbf{p}_0)^{-1}Jh\right) \leq a_\infty\right) + 0\end{aligned}\quad (46)$$

where the limit of the second term comes from the fact that $a_n = a_\infty + o(1)$.

Furthermore,

$$\begin{aligned} \mathbb{P}_{\mathbf{p}_n}(\log \Lambda_n = a_n) &\leq \mathbb{P}_{\mathbf{p}_n}(\log \Lambda_n \in [a_\infty - |a_n - a_\infty|, a_\infty + |a_n - a_\infty|]) \\ &\rightarrow 0 \end{aligned} \quad (47)$$

as again $a_n = a_\infty + o(1)$.

Finally, we can compute

$$\begin{aligned} &\mathbb{P}\left(\mathcal{N}\left(\frac{s^2}{2}h^T J^T F(\mathbf{p}_0)^{-1} J h, s^2 h^T J^T F(\mathbf{p}_0)^{-1} J h\right) \leq a_\infty\right) \\ &= \mathbb{P}\left(\mathcal{N}\left(\frac{s^2}{2}h^T J^T F(\mathbf{p}_0)^{-1} J h, s^2 h^T J^T F(\mathbf{p}_0)^{-1} J h\right) \leq -\frac{s^2}{2}h^T J^T F(\mathbf{p}_0)^{-1} J h + \sqrt{s^2 h^T J^T F(\mathbf{p}_0)^{-1} J h} Q_\alpha\right) \\ &= \mathbb{P}\left(\mathcal{N}(0, 1) \leq -\sqrt{s^2 h^T J^T F(\mathbf{p}_0)^{-1} J h} + Q_\alpha\right), \end{aligned} \quad (48)$$

which concludes the proof.

B.3. Proof of Theorem 3.2

For $p_i^{(\tau)} = \exp(z_i/\tau) / \sum_j \exp(z_j/\tau)$, we have

$$\frac{\partial p_i^{(\tau)}}{\partial z_k} = \frac{1}{\tau} p_i^{(\tau)} (\mathbf{1}\{i = k\} - p_k^{(\tau)}). \quad (49)$$

So, the full Jacobian w.r.t. the logits is the $d \times d$ matrix

$$\begin{aligned} \frac{\partial p^{(\tau)}}{\partial z} &= \frac{1}{\tau} (\text{diag}(\mathbf{p}^{(\tau)}) - \mathbf{p}^{(\tau)}(\mathbf{p}^{(\tau)})^T) \\ &= \frac{1}{\tau} \Sigma(\mathbf{p}^{(\tau)}). \end{aligned} \quad (50)$$

Since we work on reduced coordinates, we only keep the first $d - 1$ coordinates of $\mathbf{p}^{(\tau)}$. Thus the Jacobian of the reduced vector $p_{1:(d-1)}^{(\tau)}$ w.r.t. z is the $(d - 1) \times d$ matrix obtained by keeping the first $d - 1$ rows of $\Sigma(\mathbf{p}^{(\tau)})$:

$$\frac{\partial p_{1:(d-1)}^{(\tau)}}{\partial z} = \frac{1}{\tau} A(\mathbf{p}^{(\tau)}), \quad (51)$$

where $A(\mathbf{p})$ has entries $A_{c,k}(\mathbf{p}) = p_c(\mathbf{1}\{c = k\} - p_k)$ for $c \leq d - 1$.

By the chain rule, this gives

$$J^{(\tau)}(\theta) = \frac{1}{\tau} A\left(\mathbf{p}^{(\tau)}(\theta)\right) J_z(\theta). \quad (52)$$

Then we claim that we also have the identity

$$A(\mathbf{p})^T F(\mathbf{p}_{1:(d-1)})^{-1} A(\mathbf{p}) = \Sigma(\mathbf{p}). \quad (53)$$

Indeed, let us first observe that

$$F(\mathbf{p}_{1:(d-1)})^{-1} = \text{diag}(\mathbf{p}_{1:(d-1)})^{-1} + \frac{1}{p_d} \mathbf{1}\mathbf{1}^T. \quad (54)$$

This formula can be obtained with the Sherman-Morrison formula, but we only verify its validity below.

Let $D := \text{diag}(\mathbf{p}_{1:(d-1)})$ and $u := \mathbf{p}_{1:(d-1)}$, so that $F := F(\mathbf{p}_{1:(d-1)}) = D - uu^T$.

We set $M := D^{-1} + \frac{1}{p_d} \mathbf{1} \mathbf{1}^T$. We now verify that $FM = I_{d-1}$.

First,

$$DD^{-1} = I \quad (55)$$

and

$$D \left(\frac{1}{p_d} \mathbf{1} \mathbf{1}^T \right) = \frac{1}{p_d} u \mathbf{1}^T. \quad (56)$$

Next,

$$\begin{aligned} uu^T D^{-1} &= u(u^T D^{-1}) \\ &= u \mathbf{1}^T \end{aligned} \quad (57)$$

and finally

$$\begin{aligned} uu^T \left(\frac{1}{p_d} \mathbf{1} \mathbf{1}^T \right) &= \frac{1}{p_d} u(u^T \mathbf{1}) \mathbf{1}^T \\ &= \frac{1}{p_d} u(1 - p_d) \mathbf{1}^T. \end{aligned} \quad (58)$$

Therefore,

$$\begin{aligned} FM &= (D - uu^T) \left(D^{-1} + \frac{1}{p_d} \mathbf{1} \mathbf{1}^T \right) \\ &= \underbrace{DD^{-1}}_I + \underbrace{D \frac{1}{p_d} \mathbf{1} \mathbf{1}^T}_{\frac{1}{p_d} u \mathbf{1}^T} - \underbrace{uu^T D^{-1}}_{u \mathbf{1}^T} - \underbrace{uu^T \frac{1}{p_d} \mathbf{1} \mathbf{1}^T}_{\frac{1}{p_d}(1-p_d)u \mathbf{1}^T} \\ &= I + \left(\frac{1}{p_d} - 1 - \frac{1-p_d}{p_d} \right) u \mathbf{1}^T = I. \end{aligned} \quad (59)$$

Thus (54) holds.

We now compute $A^T F^{-1} A$. Using $A = [F \mid -p_d \mathbf{p}_{1:(d-1)}]$, we have

$$\begin{aligned} A^T F^{-1} A &= \begin{bmatrix} F^T \\ (-p_d \mathbf{p}_{1:(d-1)})^T \end{bmatrix} F^{-1} \begin{bmatrix} F \mid -p_d \mathbf{p}_{1:(d-1)} \end{bmatrix} \\ &= \begin{bmatrix} F & -p_d \mathbf{p}_{1:(d-1)} \\ -p_d \mathbf{p}_{1:(d-1)}^T & p_d^2 \mathbf{p}_{1:(d-1)}^T F^{-1} \mathbf{p}_{1:(d-1)} \end{bmatrix}, \end{aligned} \quad (60)$$

since F is symmetric.

It remains to compute $\mathbf{p}_{1:(d-1)}^T F^{-1} \mathbf{p}_{1:(d-1)}$ using (54):

$$\begin{aligned} \mathbf{p}_{1:(d-1)}^T F^{-1} \mathbf{p}_{1:(d-1)} &= \mathbf{p}_{1:(d-1)}^T \text{diag}(\mathbf{p}_{1:(d-1)})^{-1} \mathbf{p}_{1:(d-1)} + \frac{1}{p_d} \mathbf{p}_{1:(d-1)}^T \mathbf{1} \mathbf{1}^T \mathbf{p}_{1:(d-1)} \\ &= (1 - p_d) + \frac{(1 - p_d)^2}{p_d} \\ &= \frac{1 - p_d}{p_d}. \end{aligned} \quad (61)$$

Hence the bottom-right entry is

$$\begin{aligned} p_d^2 \mathbf{p}_{1:(d-1)}^T F^{-1} \mathbf{p}_{1:(d-1)} &= p_d^2 \frac{1 - p_d}{p_d} \\ &= p_d(1 - p_d) \\ &= p_d - p_d^2. \end{aligned} \quad (62)$$

Therefore,

$$A^T F^{-1} A = \begin{bmatrix} \text{diag}(\mathbf{p}_{1:(d-1)}) - \mathbf{p}_{1:(d-1)} \mathbf{p}_{1:(d-1)}^T & -p_d \mathbf{p}_{1:(d-1)} \\ -p_d \mathbf{p}_{1:(d-1)}^T & p_d - p_d^2 \end{bmatrix}. \quad (63)$$

which is exactly $\text{diag}(\mathbf{p}) - \mathbf{p}\mathbf{p}^T = \Sigma(p)$.

By definition,

$$\text{SNR}^2(h) = h^T \left((J^{(\tau)})^T F(\mathbf{p}_{1:(d-1)}^{(\tau)})^{-1} J^{(\tau)} \right) h. \quad (64)$$

Substituting (52) gives

$$\text{SNR}^2(h) = \frac{1}{\tau^2} h^T \left(J_z^T (A^T F^{-1} A) J_z \right) h = \frac{1}{\tau^2} h^T \left(J_z^T \Sigma(\mathbf{p}^{(\tau)}) J_z \right) h, \quad (65)$$

which is (2).

B.4. Proof of Theorem 3.3

If $k = 1$, let $\mathcal{M} = \{i^*\}$ and $\Delta = \min_{j \neq i^*} (z_{i^*} - z_j) > 0$, then for $j \neq i^*$,

$$\begin{aligned} \frac{p_j^{(\tau)}}{p_{i^*}^{(\tau)}} &= \exp \left(-\frac{z_{i^*} - z_j}{\tau} \right) \\ &\leq \exp(-\Delta/\tau), \end{aligned} \quad (66)$$

so $p_{i^*}^{(\tau)} = 1 - O(\exp(-\Delta/\tau))$ and thus $1 - \|\mathbf{p}^{(\tau)}\|_2^2 = O(\exp(-\Delta/\tau))$.

Since $\Sigma(\mathbf{p}^{(\tau)})$ is positive semidefinite and $\|\Sigma(\mathbf{p}^{(\tau)})\|_{\text{op}} \leq \text{tr}(\Sigma(\mathbf{p}^{(\tau)})) = 1 - \|\mathbf{p}^{(\tau)}\|_2^2$,

$$\begin{aligned} h^T J_z^T \Sigma(\mathbf{p}^{(\tau)}) J_z h &\leq \|J_z h\|^2 \|\Sigma(\mathbf{p}^{(\tau)})\|_{\text{op}} \\ &= O(\exp(-\Delta/\tau)). \end{aligned} \quad (67)$$

Plugging into (2) gives $\text{SNR}^2(h) \rightarrow 0$.

If $k \geq 2$, by continuity

$$h^T \left(J_z^T \Sigma(\mathbf{p}^{(\tau)}) J_z \right) h \rightarrow h^T \left(J_z^T \Sigma_{\mathcal{M}} J_z \right) h \quad (68)$$

Plugging into (2) gives $\text{SNR}^2(h) \rightarrow \infty$ if $h^T (J_z^T \Sigma_{\mathcal{M}} J_z) h \neq 0$.

B.5. Effect of the last layer

Let

$$A := J_z(\theta)^T \Sigma_{\mathcal{M}} J_z(\theta). \quad (69)$$

Since $\Sigma_{\mathcal{M}} \succeq 0$, we have $A \succeq 0$. In particular,

$$\{h \in \mathbb{S}^{q-1} : h^T A h = 0\} = \mathbb{S}^{q-1} \cap \ker(A) \quad (70)$$

has measure zero as soon as $A \neq 0$. It is therefore sufficient to show that A is not the zero matrix.

To this end, it suffices to prove that $\text{tr}(A) > 0$. Recall the Jacobian decomposition

$$J_z(\theta) = \left[W J_r(\theta_{\text{pre}}) \mid r(\theta_{\text{pre}}, x_{\text{test}})^T \otimes I_d \mid I_d \right]. \quad (71)$$

We define the head contribution to the Jacobian by

$$J_{z,\text{head}} := \left[r(\theta_{\text{pre}}, x_{\text{test}})^T \otimes I_d \mid I_d \right]. \quad (72)$$

We drop the (nonnegative) pre-head contribution, which yields

$$\begin{aligned} \text{tr}(A) &= \text{tr}(J_z^T \Sigma_{\mathcal{M}} J_z) \\ &\geq \text{tr}(J_{z,\text{head}}^T \Sigma_{\mathcal{M}} J_{z,\text{head}}), \end{aligned} \quad (73)$$

which gives

$$\text{tr}(J_{z,\text{head}}^T \Sigma_{\mathcal{M}} J_{z,\text{head}}) = \text{tr}((r^T \otimes I_d)^T \Sigma_{\mathcal{M}} (r^T \otimes I_d)) + \text{tr}(I_d^T \Sigma_{\mathcal{M}} I_d). \quad (74)$$

For the bias block,

$$\text{tr}(I_d^T \Sigma_{\mathcal{M}} I_d) = \text{tr}(\Sigma_{\mathcal{M}}) = 1 - \|\mathbf{p}_{\mathcal{M}}\|_2^2, \quad (75)$$

where we recall that $\mathbf{p}_{\mathcal{M}}$ assigns uniform mass to \mathcal{M} and zero elsewhere.

For the weight block, by the properties of the Kronecker product,

$$\begin{aligned} (r^T \otimes I_d)^T \Sigma_{\mathcal{M}} (r^T \otimes I_d) &= (r^T \otimes I_d)^T \Sigma_{\mathcal{M}} (r^T \otimes I_d) \\ &= ((r^T)^T \otimes I_d^T) \Sigma_{\mathcal{M}} (r^T \otimes I_d) \\ &= (r \otimes I_d) \Sigma_{\mathcal{M}} (r^T \otimes I_d) \\ &= ((r \otimes I_d)((1) \otimes \Sigma_{\mathcal{M}}))(r^T \otimes I_d) \\ &= (r(1) \otimes I_d \Sigma_{\mathcal{M}})(r^T \otimes I_d) \\ &= (r \otimes \Sigma_{\mathcal{M}})(r^T \otimes I_d) \\ &= (rr^T) \otimes \Sigma_{\mathcal{M}}, \end{aligned} \quad (76)$$

where $r := r(\theta_{\text{pre}}, x_{\text{test}})$, which yields

$$\begin{aligned} \text{tr}((rr^T) \otimes \Sigma_{\mathcal{M}}) &= \text{tr}(rr^T) \text{tr}(\Sigma_{\mathcal{M}}) \\ &= \|r\|_2^2 (1 - \|\mathbf{p}_{\mathcal{M}}\|_2^2). \end{aligned} \quad (77)$$

Thus,

$$\text{tr}(J_{z,\text{head}}^T \Sigma_{\mathcal{M}} J_{z,\text{head}}) = (\|r\|_2^2 + 1)(1 - \|\mathbf{p}_{\mathcal{M}}\|_2^2). \quad (78)$$

Since $\mathbf{p}_{\mathcal{M}}$ is uniform on \mathcal{M} of size k , we have $\|\mathbf{p}_{\mathcal{M}}\|_2^2 = 1/k$, and thus

$$1 - \|\mathbf{p}_{\mathcal{M}}\|_2^2 = 1 - \frac{1}{k} > 0 \quad (79)$$

for $k \geq 2$. Therefore (78) is strictly positive for $k \geq 2$, implying $\text{tr}(A) > 0$ and hence $A \neq 0$. Consequently,

$$h^T (J_z^T \Sigma_{\mathcal{M}} J_z) h \neq 0 \quad (80)$$

for almost every $h \in \mathbb{S}^{q-1}$.

In particular, if h is drawn from any non-degenerate continuous distribution on \mathbb{S}^{q-1} (or in \mathbb{R}^q and normalized), the condition holds with probability one.

B.6. Proof of Theorem 4.1

If both empirical supports equal the true support, i.e., if $\hat{S}_1 = S$ and $\hat{S}_2 = S$, then necessarily $\hat{S}_1 = \hat{S}_2$, hence \mathcal{R} cannot occur. So,

$$\mathcal{R} \subseteq \{\hat{S}_1 \neq S\} \cup \{\hat{S}_2 \neq S\}. \quad (81)$$

By the union bound,

$$\mathbb{P}_{H_0}(\mathcal{R}) \leq \mathbb{P}(\hat{S}_1 \neq S) + \mathbb{P}(\hat{S}_2 \neq S).$$

Fix $i \in \{1, 2\}$. The event $\{\hat{S}_i \neq S\}$ means that at least one element of S was never observed among the n_i draws. For each token $a \in S$, we define the indicator

$$I_{a,i} := \mathbf{1}\{a \notin \hat{S}_i\}. \quad (82)$$

Then $\{\hat{S}_i \neq S\} = \{\sum_{a \in S} I_{a,i} \geq 1\}$, so by Markov's inequality,

$$\begin{aligned} \mathbb{P}(\hat{S}_i \neq S) &= \mathbb{P}\left(\sum_{a \in S} I_{a,i} \geq 1\right) \\ &\leq \mathbb{E}\left(\sum_{a \in S} I_{a,i}\right) \\ &= \sum_{a \in S} \mathbb{P}(a \notin \hat{S}_i). \end{aligned} \quad (83)$$

Under H_0 , each draw hits a fixed token $a \in S$ with probability $1/k$, so the probability that a is never observed in n_i i.i.d. draws is

$$\mathbb{P}(a \notin \hat{S}_i) = \left(1 - \frac{1}{k}\right)^{n_i}. \quad (84)$$

So,

$$\mathbb{P}(\hat{S}_i \neq S) \leq k \left(1 - \frac{1}{k}\right)^{n_i}. \quad (85)$$

Combining this for $i = 1$ and $i = 2$ gives

$$\mathbb{P}_{H_0}(\mathcal{R}) \leq k \left(1 - \frac{1}{k}\right)^{n_1} + k \left(1 - \frac{1}{k}\right)^{n_2}. \quad (86)$$

B.7. Proof of Theorem 4.2

If the test does not reject, then all observed samples must belong to the intersection $I = S_1 \cap S_2$. In particular,

$$\mathcal{R}^c \subseteq \{\forall i, X_i \in I\} \cap \{\forall j, Y_j \in I\}. \quad (87)$$

By independence,

$$\mathbb{P}_{H_1}(\mathcal{R}^c) \leq \mathbb{P}(\forall i, X_i \in I) \mathbb{P}(\forall j, Y_j \in I). \quad (88)$$

Since $X_i \sim \text{Unif}(S_1)$ and $Y_j \sim \text{Unif}(S_2)$, $\mathbb{P}(X_i \in I) = \frac{|I|}{k_1} = p_1$ and $\mathbb{P}(Y_j \in I) = \frac{|I|}{k_2} = p_2$, which yields

$$\mathbb{P}_{H_1}(\mathcal{R}^c) \leq p_1^{n_1} p_2^{n_2}. \quad (89)$$

B.8. Proof of Theorem 4.3

We prove the lower bound using a two-point argument based on Le Cam's method.

We fix two distinct tokens $a \neq b$ in Ω and we consider the following pair of hypotheses: $H_0 : S_1^{(0)} = S_2^{(0)} = \{a, b\}$ and $H_1 : S_1^{(1)} = \{a, b\}$, $S_2^{(1)} = \{a\}$.

Let $Z := (X_1, \dots, X_n, Y_1, \dots, Y_n)$ denote the full observation, where the samples are independent and satisfy $X_i \stackrel{\text{i.i.d.}}{\sim} \text{Unif}(S_1^{(l)})$ and $Y_j \stackrel{\text{i.d.d.}}{\sim} \text{Unif}(S_2^{(l)})$ for $l \in \{0, 1\}$.

Let \mathbb{P}_0 and \mathbb{P}_1 denote the laws of Z under the null and alternative hypotheses, respectively.

Under both hypotheses, the reference support is the same, $S_1^{(0)} = S_1^{(1)} = \{a, b\}$. Consequently, the distribution of the X -sample (X_1, \dots, X_n) is identical under \mathbb{P}_0 and \mathbb{P}_1 . Since the samples are independent, the total variation distance between \mathbb{P}_0 and \mathbb{P}_1 reduces to that between the marginal distributions of the Y samples, which gives

$$\text{TV}(\mathbb{P}_0, \mathbb{P}_1) = \text{TV}((\text{Unif}\{a, b\})^{\otimes n}, \delta_a^{\otimes n}), \quad (90)$$

where $\delta_a^{\otimes n}$ denotes the point mass on the constant sequence (a, \dots, a) .

Since $\delta_a^{\otimes n}$ is supported on a single point, we have

$$\text{TV}((\text{Unif}\{a, b\})^{\otimes n}, \delta_a^{\otimes n}) = 1 - (\text{Unif}\{a, b\})^{\otimes n}(a, \dots, a). \quad (91)$$

Under $(\text{Unif}\{a, b\})^{\otimes n}$, the probability of observing (a, \dots, a) is 2^{-n} , hence

$$\text{TV}(\mathbb{P}_0, \mathbb{P}_1) = 1 - 2^{-n}, \quad (92)$$

Le Cam's inequality (Tsybakov, 2009) states that for any rejection region \mathcal{R} ,

$$\mathbb{P}_0(\mathcal{R}) + \mathbb{P}_1(\mathcal{R}^c) \geq \frac{1}{2}(1 - \text{TV}(\mathbb{P}_0, \mathbb{P}_1)). \quad (93)$$

which gives the result.

C. Derivation of Optimal Sampling Budget

In this section, we derive the optimal stopping limit m (maximum number of samples per candidate) to minimize the total query budget required to identify N Border Inputs.

C.1. Problem Setup

Let f_B be the fraction of candidate inputs that produce a Bernoulli distribution ($p = 0.5$), and let $1 - f_B$ be the fraction of inputs that produce a deterministic Dirac distribution. We define the cost function $\mathcal{L}(m)$ as the *expected number of samples required to identify a single Bernoulli candidate*. This is given by the ratio of the expected samples spent per candidate to the probability that a specific candidate is identified as a success:

$$\mathcal{L}(m) = \frac{\mathbb{E}[S_m]}{P(\text{success}|m)} \quad (94)$$

where $\mathbb{E}[S_m]$ is the expected number of samples taken per candidate given a limit m , and $P(\text{success}|m)$ is the probability a candidate is confirmed as Bernoulli within m samples.

C.2. Cost Function Derivation

A candidate is identified as a success if it is a Bernoulli distribution and we observe at least two differing outputs within m samples. The probability of failing to identify a Bernoulli distribution (observing m identical outputs) is $2 \cdot (1/2)^m = (1/2)^{m-1}$. Thus:

$$P(\text{success}|m) = f_B \left[1 - \left(\frac{1}{2} \right)^{m-1} \right] \quad (95)$$

The expected number of samples $\mathbb{E}[S_m]$ depends on the candidate type:

- **Dirac Candidates (prob. $1 - f_B$):** We always sample m times before discarding (as outputs are identical). Cost is m .
- **Bernoulli Candidates (prob. f_B):** We stop early if variation is observed. The expected number of samples is capped at m . Using the geometric series for the expected stopping time, the cost is $3 - (1/2)^{m-2}$.

Combining these terms, the total expected cost per candidate is:

$$\mathbb{E}[S_m] = (1 - f_B)m + f_B \left[3 - \left(\frac{1}{2} \right)^{m-2} \right] \quad (96)$$

Substituting into the objective function:

$$\mathcal{L}(m) = \frac{(1 - f_B)m + f_B [3 - (1/2)^{m-2}]}{f_B [1 - (1/2)^{m-1}]} \quad (97)$$

C.3. Comparison of Strategies

We compare the Naive Strategy ($m = 2$) against increasing the limit to $m = 3$.

Case $m = 2$:

$$\mathcal{L}(2) = \frac{4}{f_B} \quad (98)$$

Case $m = 3$:

$$\mathcal{L}(3) = \frac{4}{f_B} - \frac{2}{3} \quad (99)$$

Since $\mathcal{L}(3) < \mathcal{L}(2)$ holds for all $f_B \in (0, 1]$, the strategy $m = 3$ is strictly superior to $m = 2$.

Algorithm 1 B3IT Initialization

Require: Candidate inputs $\mathcal{X} = \{x_1, \dots, x_n\}$, samples per input m , target number of BIs \bar{n} , reference samples n_1 , temperature $T \approx 0$

Ensure: Border inputs \mathcal{B} , reference distributions $\{\hat{S}_1(x) : x \in \mathcal{B}\}$

- 1: // **Border Input Discovery**
- 2: $\mathcal{B} \leftarrow \emptyset$
- 3: **for** $x \in \mathcal{X}$ **do**
- 4: Sample outputs $\{y_1, \dots, y_m\} \leftarrow \text{Query}(x, T, m)$
- 5: **if** $|\{y_1, \dots, y_m\}| > 1$ **then**
- 6: $\mathcal{B} \leftarrow \mathcal{B} \cup \{x\}$
- 7: **end if**
- 8: **if** $|\mathcal{B}| \geq \bar{n}$ **then**
- 9: **break**
- 10: **end if**
- 11: **end for**
- 12: // **Reference Distribution Estimation**
- 13: **for** $x \in \mathcal{B}$ **do**
- 14: Sample reference outputs $\{y_1^{(1)}, \dots, y_{n_1}^{(1)}\} \leftarrow \text{Query}(x, T, n_1)$
- 15: $\hat{S}_1(x) \leftarrow \{y_1^{(1)}, \dots, y_{n_1}^{(1)}\}$
- 16: **end for**
- 17: **return** $\mathcal{B}, \{\hat{S}_1(x) : x \in \mathcal{B}\}$

Algorithm 2 B3IT Detection

Require: Border inputs \mathcal{B} , reference distributions $\{\hat{S}_1(x) : x \in \mathcal{B}\}$, detection samples n_2 , temperature $T \approx 0$

Ensure: Change detection decision

- 1: **for** $x \in \mathcal{B}$ **do**
- 2: Sample detection outputs $\{y_1^{(2)}, \dots, y_{n_2}^{(2)}\} \leftarrow \text{Query}(x, T, n_2)$
- 3: $\hat{S}_2(x) \leftarrow \{y_1^{(2)}, \dots, y_{n_2}^{(2)}\}$
- 4: **if** $\hat{S}_1(x) \Delta \hat{S}_2(x) \neq \emptyset$ **then**
- 5: **return** CHANGE DETECTED
- 6: **end if**
- 7: **end for**
- 8: **return** NO CHANGE DETECTED

C.4. Optimal Condition for $m = 4$

We next determine when increasing the budget to $m = 4$ becomes beneficial by solving for $\mathcal{L}(4) < \mathcal{L}(3)$. For $m = 4$, the cost function becomes:

$$\mathcal{L}(4) = \frac{4 - 1.25f_B}{0.875f_B} \quad (100)$$

Setting the inequality $\mathcal{L}(4) < \mathcal{L}(3)$:

$$\begin{aligned} \frac{4 - 1.25f_B}{0.875f_B} &< \frac{4}{f_B} - \frac{2}{3} \\ f_B &> \frac{3}{4} \end{aligned} \quad (101)$$

Thus, $m = 4$ is the optimal strategy only if the prevalence of Bernoulli candidates $f_B > 0.75$. Assuming a sparse distribution of valid candidates ($f_B \ll 0.75$), $m = 3$ is the global optimum.

D. Experimental addendum
D.1. Models used in the TinyChange Benchmark

- Qwen/Qwen2.5-0.5B-Instruct
- Qwen/Qwen2.5-7B-Instruct
- google/gemma-3-1b-it

- google/gemma-2-9b-it
- microsoft/Phi-4-mini-instruct
- mistralai/Mistral-7B-Instruct-v0.3
- deepseek-ai/DeepSeek-R1-Distill-Qwen-7B
- meta-llama/Llama-3.1-8B-Instruct
- allenai/OLMo-2-1124-7B-Instruct

D.2. Models used for the Border Input prevalence study

121 endpoints were used:

```

model: liquid/lfm-2.2-6b provider: liquid
model: liquid/lfm2-8b-alb provider: liquid
model: mistralai/mistral-nemo provider: deepinfra/fp8
model: mistralai/mistral-nemo provider: chutes/bf16
model: mistralai/minstral-3b provider: mistral
model: google/gemma-3-4b-it provider: chutes
model: nousresearch/hermes-2-pro-llama-3-8b provider: nextbit/int4
model: meta-llama/llama-guard-3-8b provider: deepinfra/bf16
model: google/gemma-3-4b-it provider: deepinfra/bf16
model: google/gemma-2-9b-it provider: nebus/fast
model: google/gemma-3-12b-it provider: chutes/bf16
model: qwen/qwen-2.5-7b-instruct provider: atlas-cloud/fp8
model: deepseek/deepseek-r1-distill-llama-70b provider: chutes/bf16
model: qwen/qwen-2.5-coder-32b-instruct provider: chutes/fp8
model: deepseek/deepseek-r1-0528-qwen3-8b provider: novita/bf16
model: microsoft/phi-4-multimodal-instruct provider: deepinfra/bf16
model: google/gemma-3-12b-it provider: novita/bf16
model: qwen/qwen3-8b provider: novita/fp8
model: thudm/glm-4.1v-9b-thinking provider: novita/bf16
model: amazon/nova-micro-v1 provider: amazon-bedrock
model: mistralai/devstral-small-2505 provider: deepinfra/bf16
model: cohore/command-r7b-12-2024 provider: cohore
model: google/gemma-3-27b-it provider: chutes/bf16
model: mistralai/minstral-3b-2512 provider: mistral
model: mistralai/minstral-8b provider: mistral
model: qwen/qwen3-235b-a22b-2507 provider: wandb/bf16
model: microsoft/phi-4 provider: nextbit/int4
model: qwen/qwen-2.5-coder-32b-instruct provider: deepinfra/fp8
model: microsoft/phi-4 provider: deepinfra/bf16
model: openai/gpt-oss-20b provider: amazon-bedrock
model: google/gemma-3-27b-it provider: deepinfra/fp8
model: google/gemma-3-27b-it provider: ncompass/fp8
model: google/gemma-3-27b-it provider: qmcloud/bf16
model: mistralai/devstral-2512 provider: chutes/fp8
model: qwen/qwen3-14b provider: chutes/bf16
model: z-ai/glm-4.5-ai provider: chutes/bf16
model: mistralai/mistral-small-3.2-24b-instruct provider: deepinfra/fp8
model: qwen/qwen3-30b-a3b provider: chutes/bf16
model: nousresearch/hermes-2-pro-llama-3-8b provider: novita/fp16
model: deepseek/deepseek-r1-distill-qwen-14b provider: novita/bf16
model: mistralai/minstral-8b-2512 provider: mistral
model: qwen/qwen3-14b provider: nextbit/int4
model: amazon/nova-lite-v1 provider: amazon-bedrock
model: mistralai/mistral-7b-instruct-v0.1 provider: cloudflare
model: mistralai/pixtral-12b provider: mistral
model: qwen/qwen3-32b provider: chutes/bf16
model: qwen/qwen3-coder-30b-a3b-instruct provider: novita/fp8
model: baidu/ernie-4.5-21b-a3b provider: novita/bf16
model: mistralai/devstral-small provider: deepinfra/fp8
model: qwen/qwen3-32b provider: deepinfra/fp8
model: qwen/qwen3-30b-a3b provider: ncompass/fp8
model: google/gemini-2.0-flash-lite-001 provider: google-vertex
model: google/gemini-2.0-flash-lite-001 provider: google-ai-studio
model: google/gemma-3-12b-it provider: crusoe/bf16
model: qwen/qwen3-30b-a3b-instruct-2507 provider: atlas-cloud/bf16
model: qwen/qwen3-30b-a3b-thinking-2507 provider: cloudflare
model: mistralai/devstral-small provider: mistral
model: mistralai/minstral-14b-2512 provider: mistral
model: mistralai/minstral-7b-instruct-v0.2 provider: together
model: qwen/qwen3-30b-a3b-instruct-2507 provider: nebus/fp8
model: qwen/qwen3-8b provider: fireworks
model: mistralai/voxtral-small-24b-2507 provider: mistral
model: mistralai/mistral-small-3.2-24b-instruct provider: mistral
model: mistralai/minstral-7b-instruct provider: together
model: meta-llama/llama-guard-2-8b provider: together
model: qwen/qwen3-coder-30b-a3b-instruct provider: nebus/fp8
model: mistralai/minstral-7b-instruct-v0.3 provider: together
model: microsoft/phi-4-reasoning-plus provider: deepinfra/bf16
model: alibaba/tongyi-depresearch-30b-a3b provider: ncompass/bf16

```

```

model: google/gemini-2.5-flash-lite provider: google-vertex
model: google/gemini-2.5-flash-lite provider: google-ai-studio
model: google/gemini-2.0-flash-001 provider: google-vertex
model: mistralai/mistral-tiny provider: mistral
model: google/gemini-2.0-flash-001 provider: google-ai-studio
model: google/gemini-2.5-flash-lite-preview-09-2025 provider: google-ai-studio
model: google/gemini-2.5-flash-lite-preview-09-2025 provider: google-vertex
model: google/gemma-3-27b-it provider: phala
model: qwen/qwen-2.5-72b-instruct provider: deepinfra/fp8
model: google/gemma-3-27b-it provider: parasail/fp8
model: deepseek/deepseek-v3.2-exp provider: atlas-cloud/fp8
model: qwen/qwen3-235b-a22b-2507 provider: deepinfra/fp8
model: deepseek/deepseek-r1-distill-qwen-32b provider: deepinfra/fp8
model: alibaba/tongyi-depresearch-30b-a3b provider: atlas-cloud/fp8
model: qwen/qwen3-v1-8b-instruct provider: novita/fp8
model: deepseek/deepseek-r1-distill-qwen-32b provider: nextbit/fp8
model: nousresearch/hermes-3-llama-3.1-70b provider: nextbit/fp8
model: nousresearch/hermes-3-llama-3.1-70b provider: deepinfra/fp8
model: mistralai/mistral-nemo provider: azure
model: qwen/qwen-2.5-7b-instruct provider: together/fp8
model: deepseek/deepseek-v3.2 provider: chutes/fp8
model: deepseek/deepseek-v3.2 provider: atlas-cloud/fp8
model: qwen/qwen-2.5-72b-instruct provider: chutes/fp8
model: qwen/qwen3-32b provider: friendli
model: deepseek/deepseek-v3.2 provider: phala
model: deepseek/deepseek-v3.2-exp provider: novita/fp8
model: deepseek/deepseek-v3.2-speciale provider: chutes/fp8
model: mistralai/mistral-small-3.2-24b-instruct provider: parasail/bf16
model: deepseek/deepseek-v3.2 provider: deepseek
model: qwen/qwen3-235b-a22b-thinking-2507 provider: chutes/bf16
model: qwen/qwen3-235b-a22b provider: deepinfra/fp8
model: deepseek/deepseek-v3.2 provider: baseten/fp4
model: openai/gpt-4o-mini-2024-07-18 provider: openai
model: qwen/qwen3-v1-30b-a3b-instruct provider: deepinfra/fp8
model: openai/gpt-4o-mini provider: azure
model: openai/gpt-oss-120b provider: amazon-bedrock
model: qwen/qwen3-v1-30b-a3b-instruct provider: fireworks
model: qwen/qwen3-30b-a3b provider: fireworks
model: openai/gpt-4o-mini provider: openai
model: cohere/command-r-08-2024 provider: cohere
model: qwen/qwen3-30b-a3b provider: friendli
model: mistralai/mistral-saba provider: mistral
model: qwen/qwen-2.5-72b-instruct provider: hyperbolic/bf16
model: thedrummer/unslopnemo-12b provider: nextbit/fp8
model: qwen/qwen3-235b-a22b provider: together/fp8
model: qwen/qwen3-v1-8b-instruct provider: together
model: qwen/qwen3-32b provider: groq
model: qwen/qwen3-next-80b-a3b-instruct provider: chutes/bf16
model: deepseek/deepseek-chat-v3.1 provider: samanova/high-throughput
model: mistralai/mistral-small-3.1-24b-instruct provider: cloudflare
model: deepseek/deepseek-chat-v3.1 provider: chutes/fp8
model: qwen/qwen3-30b-a3b-instruct-2507 provider: alibaba

```

D.3. Endpoints used for B3IT tracking

The following 93 endpoints were used:

```

model: mistralai/mistral-nemo provider: chutes/bf16
model: mistralai/mistral-nemo provider: deepinfra/fp8
model: mistralai/ministral-3b provider: mistral
model: google/gemma-3-4b-it provider: chutes
model: nousresearch/hermes-2-pro-llama-3-8b provider: nextbit/int4
model: google/gemma-2-9b-it provider: nebulus/fast
model: google/gemma-3-4b-it provider: deepinfra/bf16
model: google/gemma-3-12b-it provider: chutes/bf16
model: deepseek/deepseek-r1-distill-llama-70b provider: chutes/bf16
model: qwen/qwen-2.5-coder-32b-instruct provider: chutes/fp8
model: google/gemma-3-12b-it provider: novita/bf16
model: liquid/lfm-2.2-6b provider: liquid
model: liquid/lfm2-8b-alb provider: liquid
model: microsoft/phi-4-multimodal-instruct provider: deepinfra/bf16
model: google/gemma-3-12b-it provider: deepinfra/bf16
model: thudm/glm-4.1v-9b-thinking provider: novita/bf16
model: amazon/nova-micro-v1 provider: amazon-bedrock
model: mistralai/devstral-small-2505 provider: deepinfra/bf16
model: cohere/command-r7b-12-2024 provider: cohere
model: google/gemma-3-27b-it provider: chutes/bf16
model: microsoft/phi-4 provider: nextbit/int4
model: mistralai/ministral-3b-2512 provider: mistral
model: mistralai/ministral-8b provider: mistral
model: qwen/qwen3-235b-a22b-2507 provider: wandb/bf16
model: z-ai/glm-4-32b provider: z-ai
model: microsoft/phi-4 provider: deepinfra/bf16
model: openai/gpt-oss-20b provider: amazon-bedrock
model: google/gemma-3-27b-it provider: ncompass/fp8
model: qwen/qwen3-14b provider: chutes/bf16
model: z-ai/glm-4.5-air provider: chutes/bf16
model: nousresearch/hermes-2-pro-llama-3-8b provider: novita/fp16
model: amazon/nova-lite-v1 provider: amazon-bedrock

```

```

model: mistralai/minstral-8b-2512 provider: mistral
model: mistralai/mistral-7b-instruct-v0.1 provider: cloudflare
model: mistralai/mistral-nemo provider: mistral
model: mistralai/pixtral-12b provider: mistral
model: qwen/qwen3-14b provider: nextbit/int4
model: qwen/qwen3-14b provider: deepinfra/fp8
model: baidu/ernie-4.5-21b-a3b provider: novita/bf16
model: google/gemini-3-12b-it provider: crusoe/bf16
model: qwen/qwen3-30b-a3b-thinking-2507 provider: cloudflare
model: meta-llama/llama-guard-2-8b provider: together
model: mistralai/mistral-7b-instruct-v0.3 provider: together
model: qwen/qwen3-32b provider: nebulis/base
model: qwen/qwen3-8b provider: fireworks
model: alibaba/tongyi-deepresearch-30b-a3b provider: ncompass/bf16
model: google/gemini-2.5-flash-lite-preview-09-2025 provider: google-ai-studio
model: google/gemini-2.5-flash-lite-preview-09-2025 provider: google-vertex
model: google/gemma-3-27b-it provider: phala
model: mistralai/mistral-nemo provider: azure
model: deepseek/deepseek-v3.2 provider: atlas-cloud/fp8
model: qwen/qwen3-32b provider: friendli
model: deepseek/deepseek-v3.2 provider: phala
model: mistralai/mistral-small-3.2-24b-instruct provider: parasail/bf16
model: deepseek/deepseek-v3.2 provider: deepseek
model: deepseek/deepseek-v3.2 provider: parasail/fp8
model: cohere/command-r-08-2024 provider: cohere
model: openai/gpt-4o-mini provider: azure
model: openai/gpt-4o-mini provider: openai
model: openai/gpt-oss-120b provider: amazon-bedrock
model: qwen/qwen3-30b-a3b provider: friendli
model: qwen/qwen3-vl-30b-a3b-instruct provider: fireworks
model: qwen/qwen-2.5-72b-instruct provider: hyperbolic/bf16
model: qwen/qwen3-32b provider: groq
model: qwen/qwen3-235b-a22b-2507 provider: crusoe/bf16
model: kwaipilot/kat-coder-pro provider: streamlake/fp16
model: deepseek/deepseek-chat-v3-0324 provider: atlas-cloud/fp8
model: qwen/qwen3-vl-235b-a22b-instruct provider: fireworks
model: qwen/qwen3-32b provider: cerebras
model: qwen/qwen3-32b provider: samanova
model: prime-intellect/intellect-3 provider: nebulis/fp8
model: deepseek/deepseek-chat-v3-0324 provider: baseten/fp8
model: qwen/qwen3-235b-a22b-2507 provider: cerebras
model: deepseek/deepseek-chat-v3-0324 provider: fireworks
model: qwen/qwen3-coder provider: baseten/fp8
model: deepseek/deepseek-chat-v3.1 provider: samanova/fp8
model: mistralai/devstral-medium provider: mistral
model: z-ai/glm-4.6 provider: mancer/fp8
model: z-ai/glm-4.7 provider: mancer/fp8
model: deepseek/deepseek-chat-v3-0324 provider: hyperbolic/fp8
model: z-ai/glm-4.5 provider: wandb/bf16
model: z-ai/glm-4.6:exacto provider: z-ai
model: moonshotai/kimi-k2-0905:exacto provider: moonshotai
model: moonshotai/kimi-k2-thinking provider: moonshotai/int4
model: google/gemini-3-flash-preview provider: google-ai-studio
model: google/gemini-3-flash-preview provider: google-vertex
model: relace/relace-search provider: relace/bf16
model: anthropic/clause-haiku-4.5 provider: anthropic
model: meta-llama/llama-3.1-405b provider: hyperbolic/bf16
model: inflection/inflection-3-pi provider: inflection
model: openai/gpt-4o provider: openai
model: anthropic/clause-sonnet-4.5 provider: amazon-bedrock
model: anthropic/clause-sonnet-4.5 provider: anthropic

```

D.4. Selecting minimum-length prompts

We are looking for prompt strings that are encoded into a minimal number of tokens. To find them, we download 11 tokenizers, representing 47 models from the Deepseek, Qwen, Gemma, LLaMA, Phi, Mistral, and GPT-OSS series. For each tokenizer, we select unique decoded tokens from its vocabulary, replacing the special characters U+0120 and U+2581 with a space, skipping special tokens and tokens that get encoded into more than 2 token IDs (which can happen due to weird representation of partial UTF-8 characters, itself due to BPE tokenization). For models with an unknown tokenizer (e.g. the Claude model series), we use a proxy tokenizer where the prompts are in order of decreasing frequency among the known tokenizers (prompts that many tokenizers encode as a single token are more likely to be encoded as a single token by an unknown tokenizer).

D.5. TinyChange experimental parameters and methodology

For all methods, models, variants, and method parameters, all prompts were initially sampled 5,000 times each. 1,000 test statistic were subsequently generated, using random sampling in the prompts (where appropriate) and in the samples for each prompt. Unless otherwise specified, the number of detection samples is 10. Error bars in Figures 3 and 7 come from 250 bootstraps holding everything fixed except the test statistics for each condition, which are resampled with replacement. 95% confidence intervals are extracted from these bootstraps.

D.6. Parameter sweeps

Figure 6 shows the hyperparameters that were varied for each of the baselines.

For the TinyChange difficulty scale plots, we kept the following hyperparameters, always keeping 50 reference samples/prompt:

- B3IT: 5 prompts, 3 detection samples/prompt (sweep: see Figure 1)
- MET: 25 prompts, 5 output tokens (10 detection samples/prompt)
- MMLU-ALG: 100 prompts (10 detection samples/prompt)
- LT: 10 detection samples/prompt (1 prompt)

D.7. Misc

Note on OLMo. For OLMo-2-1124-7B in our in-vitro experiments, the first token was the same for all inputs. We therefore generated two tokens and retained the second. This workaround slightly increases cost, but preserves the method.

D.8. Full TinyChange difficulty scales

Figure 7 shows four more difficulty scales, in addition to the fine-tuning one presented in the main paper.

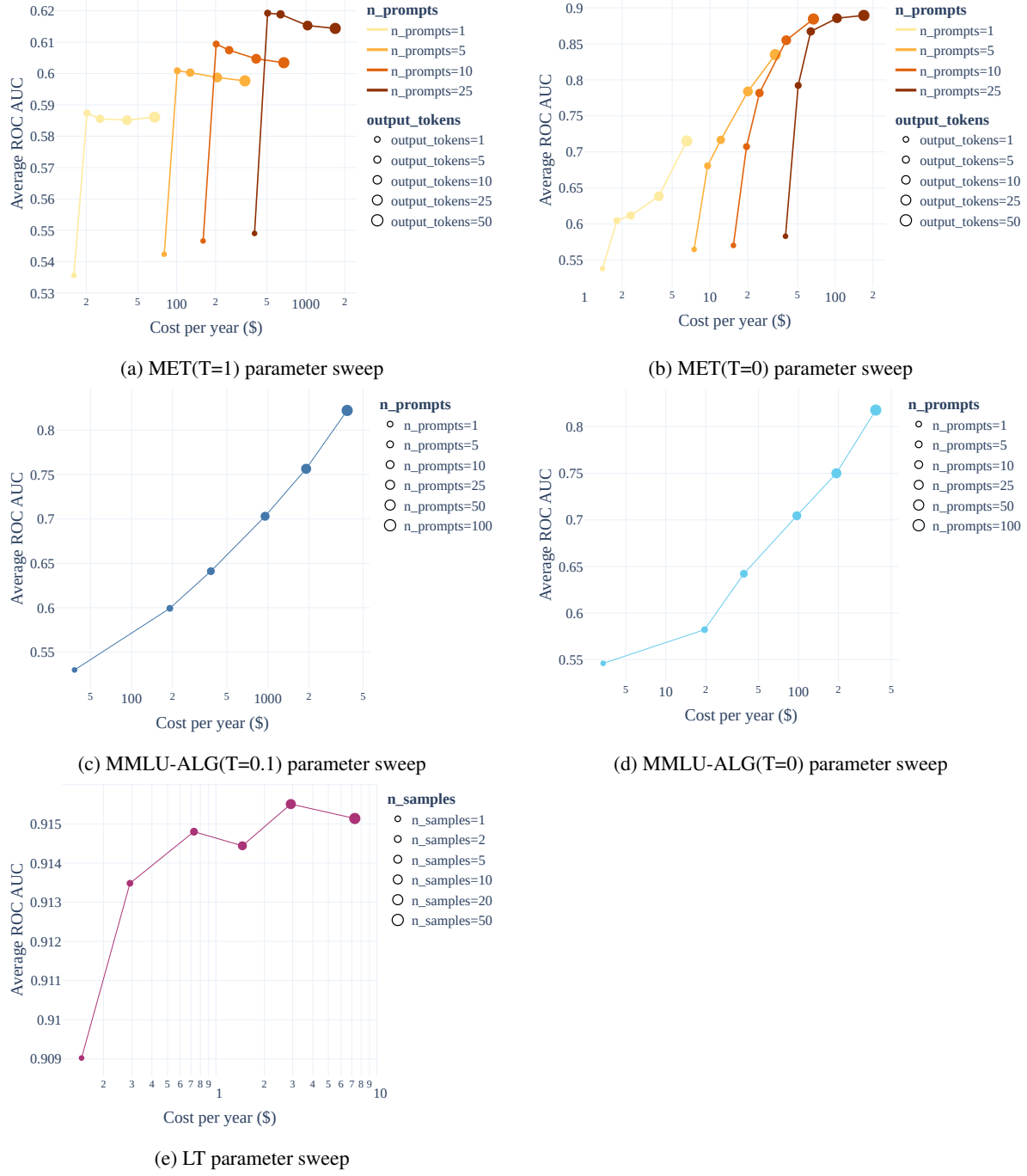


Figure 6. Detection performance on the TinyChange difficulty scales, for various perturbations.

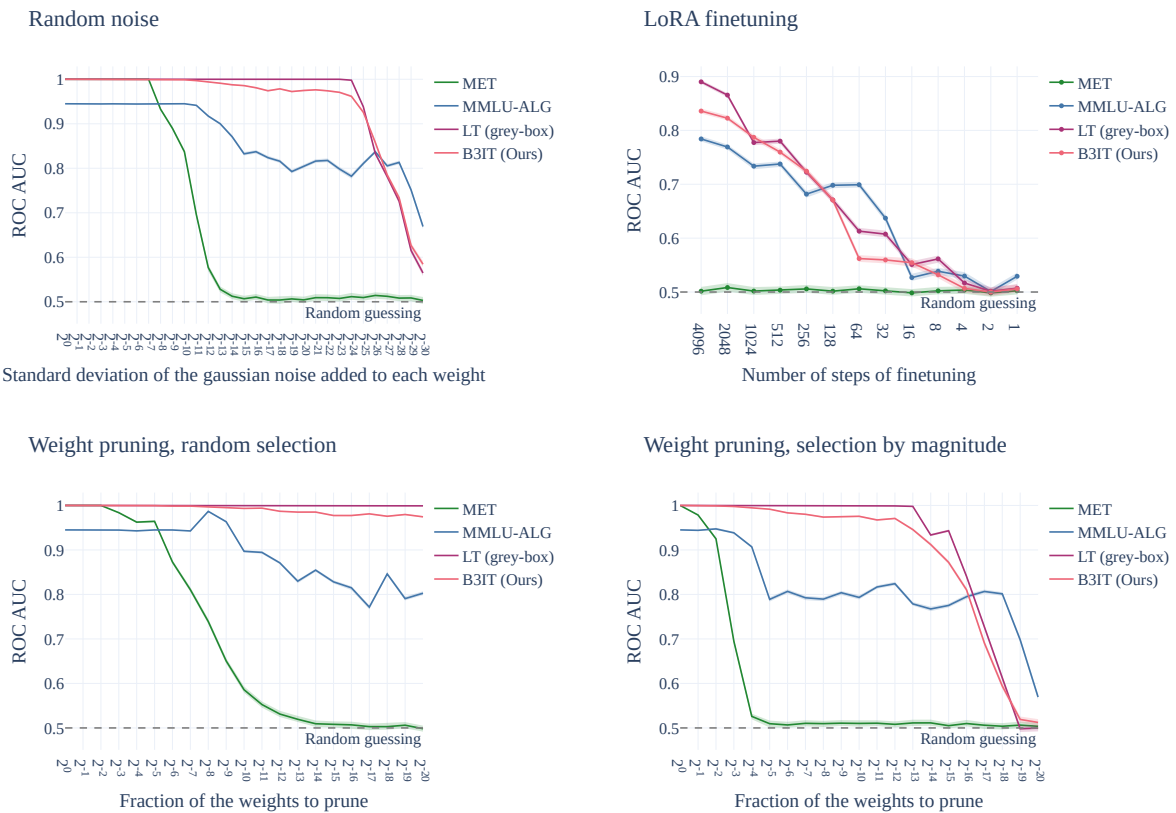


Figure 7. Detection performance on the TinyChange difficulty scales, for various perturbations.